Draft version February 1, 2008
Preprint typeset using LaTeX style emulateapj v. 10/09/06

arXiv:0707.1523v2 [astro-ph] 16 Jul 2007

AGES AND ABUNDANCES OF RED SEQUENCE GALAXIES AS A FUNCTION OF LINER EMISSION LINE STRENGTH

Genevieve J. Graves[1], S. M. Faber[1], Ricardo P. Schiavon[2], & Renbin Yan[3]

Draft version February 1, 2008

ABSTRACT

Although the spectrum of a prototypical early-type galaxy is assumed to lack emission lines, a substantial fraction (likely as high as 30%) of nearby red sequence galaxy spectra contain emission lines with line ratios characteristic of low ionization nuclear emission-line regions (LINERs). We use spectra of ~ 6000 galaxies from the Sloan Digital Sky Survey (SDSS) in a narrow redshift slice ($0.06 < z < 0.08$) to compare the stellar populations of red sequence galaxies with and without LINER-like emission. The spectra are binned by internal velocity dispersion (σ) and by emission properties to produce high S/N stacked spectra. The recent stellar population models of R. Schiavon (2006) make it possible to measure ages, [Fe/H], and individual elemental abundance ratios [Mg/Fe], [C/Fe], [N/Fe], and [Ca/Fe] for each of the stacked spectra. We find that red sequence galaxies with strong LINER-like emission are systematically 2–3.5 Gyr (10–40%) younger than their emission-free counterparts at the same σ. This suggests a connection between the mechanism powering the emission (whether AGN, post-AGB stars, shocks, or cooling flows) and more recent star formation in the galaxy. We find that mean stellar age and [Fe/H] increase with σ for all galaxies. Elemental abundance [Mg/Fe] increases modestly with σ in agreement with previous results, and [C/Fe] and [N/Fe] increase more strongly with σ than does [Mg/Fe]. [Ca/Fe] appears to be roughly solar for all galaxies. At fixed σ galaxies with fainter r-band luminosities have lower [Fe/H] and older ages but similar abundance ratios compared to brighter galaxies.

Subject headings: galaxies: abundances, galaxies: elliptical and lenticular

1. INTRODUCTION

An important recent result in the field of galaxy evolution is the build-up of the red sequence between $z = 1$ and the present. The red sequence luminosity function determined by the COMBO-17 survey (Bell et al. 2004) shows an accumulation of massive red galaxies since $z = 1$. This result was confirmed by Faber et al. (2006) using combined data from COMBO-17 and the DEEP2 redshift survey. Faber et al. (2006) contrasted the evolving luminosity function of red galaxies with the luminosity function of massive blue galaxies, which remains roughly constant over the same epoch. With so much transition in the relatively recent past, there should be visible evidence of recent red-galaxy creation in the local universe; that is, nearby galaxy samples might contain galaxies that are currently evolving onto the red sequence, as well as recent red sequence arrivals.

Stellar population models predict that once a galaxy has ceased to form stars it will move to the red sequence rapidly. A galaxy whose star formation is quenched suddenly after a history of continuous constant star formation will arrive on the red sequence within ~ 400 Myr, while a galaxy that experiences a substantial burst of star formation before quenching will take only ~ 1 Gyr to become red (Harker et al. 2006). The red sequence may therefore include galaxies which contain a fractional population of stars with young ages. Under the possibly more reasonable assumption of star formation that declines with time, the fraction of young stars will be smaller, will contribute less to the total galaxy light, and presumably the galaxy will move to the red sequence more rapidly.

Recently, Yi et al. (2005), Kaviraj et al. (2006), and Schawinski et al. (2006) have used near-ultraviolet (NUV) photometry from the GALEX Medium Imaging Survey in conjunction with Sloan Digital Sky Survey (SDSS) optical photometry to examine the colors of early-type galaxies. They show that morphologically selected early-type galaxies have uniformly red optical colors but exhibit a wide range of NUV-optical colors. According to their analysis, the observed blue NUV-optical colors in some early-type galaxies are indicative of low levels of residual star formation; they use Bruzual & Charlot (2003) stellar population models to demonstrate that blue *NUV*-optical colors are sensitive to very low levels of recent star formation and determine that at least 30% of red sequence galaxies have 1–3% of their mass in young (age < 1 Gyr) stars, with typical ages for the young component of 300–500 Myr.

Although the NUV-optical colors of these morphologically selected galaxies show signs of recent star formation, the galaxies in their sample lack optical emission lines, almost without exception. Kaviraj et al. (2006) show that their morphological selection criterion removes virtually all galaxies with emission lines characteristic of HII regions. In addition, they exclude all galaxies with emission lines characteristic of active galactic nuclei (AGN) and low ionization nuclear emission regions (LINERs), using the criterion established by Kauffmann et al. (2003). This is to remove from the sample galaxies that might have substantial ultraviolet (UV) light generated by a source other than the stars. However, by excluding all galaxies with AGN-like emission lines, they may have removed many red sequence galaxies from their

---

[1] UCO/Lick Observatory, University of California, Santa Cruz
[2] University of Virigina
[3] University of California, Berkeley

sample which are not forming stars. These galaxies could include many of the most recent arrivals on the red sequence.

Kauffmann et al. (2003) show that the host galaxies of luminous ([OIII]λ5007 emission line luminosities in excess of $10^7 L_\odot$) AGN appear to be young or post-starburst systems, while those of low-luminosity active nuclei (a category dominated by LINERs in their sample) have morphologies and stellar populations that are comparable to those of early-type galaxies with no emission. Recently, Yan et al. (2006) have shown that up to 30% of red sequence galaxies in the SDSS have emission lines, with line ratios characteristic of LINERs. Another $\sim 50\%$ of the red sequence consists of "quiescent" galaxies with no detectable emission, while the remaining $\sim 20\%$ are divided among Seyferts, dusty star-forming galaxies, and Transition Objects, which likely contain both Seyfert and HII region emission (Yan et al. 2006). A significant fraction of the red sequence population therefore consists of galaxies with optical line emission, although these galaxies are not necessarily forming stars. These galaxies are often systematically excluded from stellar population analysis of red sequence or early-type galaxies, even though they are a large class of objects and may harbor clues to the evolution of galaxies onto the red sequence.

This paper presents a stellar population analysis of red sequence galaxies, including both quiescent galaxies with no emission and those with LINER-like emission. The fact that galaxies with LINER-like emission lines make up 30% of the red sequence, in addition to having morphologies and stellar populations that appear to be consistent with the larger population of early-type galaxies generally, justifies a stellar population analysis performed in parallel with quiescent red sequence galaxies. Also, if LINERs are genuinely active nuclei and if their host galaxies form the low luminosity end of the AGN host galaxy sequence described in Kauffmann et al. (2003), these galaxies with LINER-like emission may be candidates for "post post-starburst" systems that have recently stopped forming stars and moved onto the red sequence. Signs of such recent quenching could then be detected through a careful differential stellar population analysis of LINERs versus non-LINERs.

There is still no consensus on the physical mechanism that powers LINER emission. Possibilities include photoionization by a central AGN accretion disk as in higher ionization Seyferts (Ferland & Netzer 1983, Halpern & Steiner 1983), excitation through shocks (as in the models of Dopita & Sutherland 1995), accretion of warm gas in cooling flows (e.g. Heckman 1981), or photoionization by post asymptotic giant branch (AGB) stars in either old (Binette et al. 1994) or young (Taniguchi, Shioya, & Murayama 2000) stellar populations. This topic is covered by the Filippenko (2003) review, which includes a nice summary of these mechanisms.

There are clearly LINERs whose emission is strongly dominated by low luminosity cental AGN, identified by either a central non-stellar source (an X-ray or UV point source, or a compact radio core) or by a signature of AGN accretion (broad line emission or even double-peaked broad Hα emission). Examples of each of these are referenced in Filippenko (2003). However, there is also substantial evidence for ionized gas in early type galaxies that extends *multiple kiloparsecs* from the galaxy center, as shown in narrow-band imaging of early-type galaxies (e.g., Goudfrooij et al. 1994, Macchetto et al. 1996) and more recently in the SAURON integral field unit spectroscopy of elliptical and lenticular galaxies (Sarzi et al. 2006). These studies imply that a large fraction of luminous elliptical galaxies contain *distributed* ionized gas with optical emission line ratios that are characteristic of LINERs. We must be careful with terminology, since the original definition of the term LINER (Heckman 1980) required that the emission be nuclear ("low ionization *nuclear* emission-line region"). These galaxies are therefore not nuclear LINERs, but they do exhibit emission with LINER-like ratios. We shall therefore refer to them as "LINER-like" galaxies, without any assumption about the spatial distribution of the ionized gas within the galaxy or the ionization mechanism. From SDSS data alone, whose spectral fibers cover a substantial portion of the galaxy, it is not possible to decide whether any given galaxy is a classic AGN LINER, an extended LINER-like galaxy, or some combination of the two.

The fact that LINER-like emission is common in red sequence galaxies prompts many questions: is it an evolutionary phase that all early-type galaxies pass through? Do galaxies pass through this stage more than once? Perhaps many times? Is it a cyclical process? Is the gas external in origin, as might be suggested by the kinematic decoupling of gas and stars seen by Caon, Macchetto, & Pastoriza (2000) and Sarzi et al. (2006), or is it produced by mass-loss from stars within the galaxy? What is the relation, if any, between the central AGN LINER emission and the more extended LINER-like emission? In this paper, we seek to address some of these questions by examining the stellar populations of the host galaxies to determine whether or not the existence of LINER-like emission in a red sequence galaxy is related to its star formation history.

Past stellar population analysis of early-type or red sequence galaxies has tended to either exclude all galaxies with emission (e.g., Nelan et al. 2005 and Bernardi et al. 2003b) or to include galaxies with weak LINER-like emission in the main sample. In the latter case, authors have made a correction for Balmer line emission infill using an empirical correction based on the strength of the [OIII]λ5007 (e.g., González 1993, Trager et al. 2000a, Rampazzo et al. 2005) or [OII]λ3727 (e.g., Schiavon et al. 2006) emission lines, or else restrict themselves to using higher-order Balmer lines such as Hγ and Hδ, where contamination from emission is less.

In this work, we analyze galaxies with and without LINER-like emission in parallel, in order to contrast their stellar population properties. LINER-like nebulae produce only modest quantities of Balmer emission, and that emission is well-characterized (due to the selection process described in §2.2). This allows us to make accurate Balmer infill corrections for multiple Balmer lines and to compare results. In order to obtain very high signal to noise (S/N) spectra for the stellar population analysis, we stack several hundred similar galaxies to produce highly accurate determinations of the mean stellar population properties of the galaxies that go into each composite. We use the new single stellar population (SSP) models of Schiavon (2007), which allow the determination of not only mean ages and total metallicities, but of several individual elemental abundances as well; iron, magnesium, carbon, nitrogen, and calcium are all separately determined. Section 2 presents the data sample, the criteria for grouping similar galaxies used to construct the composite spectra, and the procedure used to correct for Balmer emission infill in the LINER-like galaxies. Section 3 gives results of our line strength measurements as a function of galaxies properties. Section 4 describes the stellar population modeling process and important caveats, then §5 uses SSP models to interpret the line strength measurements in terms of stellar population properties. In §6, we discuss the implications of our results on the possible source of the LINER-like emission in red sequence galaxies, and §7 summarizes our conclusions.

2. DATA

This paper presents an analysis of red sequence galaxy spectra from the Sloan Digital Sky Survey (SDSS), a massive imaging and spectroscopic survey conducted at the Apache Point Observatory with a dedicated 2.5 m telescope. The SDSS has imaged more than one quarter of the sky in five filter bands: *u, g, r, i,* and *z* (Fukugita et al. 1996, Stoughton et al. 2002). The survey has also obtained spectroscopic observations of over one million galaxies and quasars using a purpose-built dual fiber spectrograph, with resolution $R = \lambda/\Delta\lambda \approx 1800$, wavelength coverage $\lambda = 3800$–9200Å, and fiber diameter $d = 3''$. The data presented in this paper are taken as part of the SDSS main galaxy sample, which includes over 500,000 galaxies with redshifts $0.00 \leq z \leq 0.30$. The main galaxy sample is selected to include galaxies brighter than $r < 17.77$.

The following imaging and spectroscopic parameters for each galaxy were taken from the NYU Value Added Catalog (Blanton et al. 2004, Adelman-McCarthy et al. 2005), Data Release 4 (DR4): redshift z, velocity dispersion $\sigma_{\rm fib}$ as measured in the SDSS fiber spectrum, *ugriz* fluxes measured in the SDSS flux units "maggies" (see Blanton et al. 2004), and median S/N per Å for each spectrum. The *ugriz* fluxes were converted to absolute magnitudes assuming standard ΛCDM cosmology ($\Omega_\Lambda = 0.7$, $\Omega_m = 0.3$), with a Hubble constant of $H_0 = 70$ km s^{-1} Mpc^{-1}. The magnitudes were then K-corrected to $z = 0.1$ using Mike Blanton's *kcorrect* code, v. 3_2 (Blanton et al. 2003a). We chose to K-correct to $z = 0.1$ both to enable easy comparison with colors and magnitudes for SDSS galaxies in Blanton et al. (2003b) and because we limited our galaxy sample to galaxies with $0.06 < z < 0.08$ (see §2.1); the K-correction to $z = 0.1$ is small and therefore any errors due to uncertainty in the K-correction are minimized. Throughout this paper, all magnitudes and colors are quoted at $z = 0.1$, unless otherwise noted.

These values were supplemented with the following measurements from the SDSS DR4 Catalog Archive Server: the best-fit deVaucouleurs radius (r_e) and axis ratio (b/a). Our analysis also uses emission line equivalent widths (EWs) for Hα, Hβ, [OII]λ3727, [OIII]λ5007, [OI]λ6300, and [NII]λ6583 measured in SDSS DR4 galaxies by Yan et al. (2006), with the zeropoint corrections defined in their Table B3. Before making their emission line measurements, Yan et al. fit and subtract off a stellar absorption line template spectrum to obtain good measurements of even those emission lines that fall on top of stellar absorption features. The interested reader should consult their paper for further details on this process.

2.1. *Sample Selection*

The sample is chosen to match the selection criteria of the Yan et al. (2006) magnitude limited sample; objects are from the SDSS main galaxy sample and are spectroscopically confirmed to be galaxies. We then limit the sample to a narrow range in redshift, $0.06 < z < 0.08$, making this magnitude-limited sample roughly volume-limited and minimizing the impact of evolution on this analysis. The 1.5″ SDSS spectral fiber radius corresponds to 1.7–2.3 kpc in this redshift range.

The aim of this work is to study red sequence galaxies with no active star formation. We use two selection criteria to select galaxies which are not currently forming stars: a color cut (described below) and the emission line properties of the galaxies. Yan et al. (2006) demonstrated that the distribution of [OII] to Hα emission line EW ratios is bimodal such that some emission line galaxies have strong Hα emission but relatively weak [OII] emission while others have strong [OII] and weak Hα. This is best seen in a plot of log EW(Hα) vs. log EW([OII]), as in Figure 1a (see also Yan et al. 2006, Figure 2).

They showed that the left peak with high EW([OII]) and low EW(Hα) (they call these "High-[OII]/Hα" galaxies) is dominated by red sequence galaxies, whereas the right peak with larger EW(Hα) ("Low-[OII]/Hα" galaxies) is dominated by blue galaxies. This led them to explore the possibility that the High-[OII]/Hα galaxies are star-forming systems while the Low-[OII]/Hα galaxies contain emission that is not powered by star formation. They confirm this hypothesis through the use of line ratio classification diagrams first proposed by Baldwin, Phillips, & Terlevich (1981) and commonly known as "BPT diagrams".

Following Yan et al. (2006), we define red sequence galaxies as those with

$$^{0.1}(g-r) > -0.025(\,^{0.1}M_r - 5\log h) + 0.42, \quad (1)$$

here with $h = 0.70$. This includes 22,501 galaxies in the chosen redshift range. This color cut is shown in Figure 1c as the dashed line. The color cut has been chosen to be conservative and excludes galaxies that lie in the "valley" between the red sequence and the bulk of blue galaxies. On the red sequence, we use Hα and [OII] EWs to characterize galaxies according to their emission line properties. We use the Yan et al. (2006) relation

$$\mathrm{EW([O\,II])} > 5\mathrm{EW(H\alpha)} - 7, \quad (2)$$

to separate High-[OII]/Hα from Low-[OII]/Hα galaxies. This dividing line is shown as the solid line in Figures 1a and 1b. Figure 1a shows the same information as Figure 1b, but with linear axes. The latter format does not highlight the bimodality as clearly but is a more natural way to examine the cut used to define the High-[OII]/Hα sample.

To confirm that the High-[OII]/Hα objects are not star forming galaxies, Figure 2 shows BPT diagrams of emission line galaxies in the redshift range $0.06 < z < 0.08$. Red points show the red sequence High-[OII]/Hα objects as defined above; black points show all other emission-line galaxies. Only galaxies with a $\geq 3\sigma$ detection in all lines are shown on each plot. Panel (b) contains fewer objects than (a) because [OI]λ6300 is a weak line and undetected in 2/3 of the High-[OII]/Hα and 1/2 of all other galaxies shown in (a). The solid lines in each panel show the standard classification scheme dividing Seyferts, LINERs, and star forming galaxies. The dotted lines show the Kewley et al. (2001) division between star forming galaxies and active nuclei; the dashed line in (a) shows the division used by Kauffmann et al. (2003). The dash-dot line in (b) shows the Ho, Filippenko, & Sargent (1997) division between LINERs and transition objects (TOs). Based on the Kauffmann et al. (2003) division between star forming galaxies and active nuclei, the standard division between LINERs and Seyferts, and the Ho, Filippenko, & Sargent (1997) division between LINERs and TOs, the red sequence High-[OII]/Hα galaxies consist of 88.4% LINERs, 8.6% TOs, 1.9% Seyferts, and 1.1% star forming galaxies. Most of the High-[OII]/Hα objects classified as TOs lie very near the division between LINERs and TOs, well within the typical errors, and are not convincingly a separate class of objects. There are High-[OII]/Hα galaxies that are not shown here because their Hβ, [OIII]λ5007, [OI]λ6300, and/or [NII]λ6583 emission lines are weaker than 3σ detections, but they are assumed to possess the same underlying emission line properties as those shown.

The analysis in this paper uses two samples of galaxies classified by their [OII] and Hα emission lines: galaxies with neither Hα nor [OII] detected (at the 2σ level) and High-[OII]/Hα galaxies with both lines detected. We shall hereafter refer to these as "quiescent" and "LINER-like" galaxies respectively. The color distributions of these samples are similar and concentrated on the red sequence. Figure 1d shows CMDs of the quiescent and LINER-like galaxies, with the color cut defining the red sequence overplotted as the dashed line (as in Figure 1c). While the colors of the LINER-like and quiescent galaxies are similar, the luminosity distribution is clearly different. This is partially a selection effect; the LINER-like galaxies are required to have both [OII] and Hα detected at the 2σ level, thus fainter galaxies with lower S/N spectra are less likely to meet the selection criteria. Taking this effect into account, there still appears to be a decline in the fraction of red sequence LINER-like galaxies at faint magnitudes. This will be explored in more detail in future work. Only galaxies redder than the dashed line of Figures 1c-d are included in our sample. Spectra of the quiescent and LINER-like red sequence galaxies were downloaded from the SDSS Data Archive Server (http://das.sdss.org).

As defined, our sample of galaxies contains overlap with the sample of AGNs and their hosts described by Kauffmann et al. (2003). They select galaxies on the basis of their log([NII]λ6583/Hα) and log([OIII]λ3727/Hβ) ratios, including galaxies that are classified as Seyferts by the criteria of Ho, Filippenko, & Sargent (1997), as well as LINERs and some Transition Objects. They claim that all of these objects harbor AGN of some kind, and divide their sample into low-luminosity and high-luminosity AGN, with the dividing line at log $L_{[\mathrm{OIII}]}/L_{\odot} = 7.0$. Careful study of their Figure 3 reveals that at least 85% of the objects that they classify as LINERs fall into their low-luminosity AGN sample, while only $\sim$ 20% of their Seyferts fall into this sample. Comparisons to the results of Kauffmann et al. (2003) are therefore most appropriate between our sample and their "low-luminosity AGN" sample. However, they apply no color criterion to their selection of AGN hosts. Of the galaxies in our Figure 2 which meet the Kauffmann et al. (2003) definition of AGN, 55% are bluer than our red sequence cut-off and 37% meet the more conservative color criterion for blue galaxies in Yan et al. (2006). The Kauffmann et al. (2003) sample clearly includes many more young (and possibly actively star forming) galaxies than our sample. Their analysis of other properties of the host galaxies suggest that the hosts of strong AGN are young galaxies but that the hosts of their low-luminosity AGN sample are similar to early-type galaxies, so many or most of these blue galaxies may be in their high-luminosity AGN sample. However, their low-luminosity AGN sample is still likely to contain a significant fraction of galaxies bluer than any present in our analysis.

2.2. *Emission Infill Correction*

Our analysis uses the strength of the stellar Hβ, Hγ, and Hδ absorption features, in conjunction with metal lines, to measure SSP ages for the galaxies in our sample. In the LINER-like galaxies, stellar Balmer line absorption will be partially or completely filled in by emission from the ionized gas within the galaxy. This infill severely impacts stellar population analysis, and a correction must be made. If we use the Hα and Hβ emission line strengths measured by Yan et al. (2006) to make an emission infill correction, we merely recover the Balmer absorption line strengths of their subtracted absorption line spectral template, and further stellar population modeling will be meaningless. González (1993) defined an Hβ infill correction based on the EW of [OIII]λ5007 emission, which has been used (sometimes in modified form) by many other groups. Trager et al. (2000a) use $\Delta\mathrm{H}\beta = 0.7$ EW([OIII]) which, assuming the continuum level is similar at Hβ and [OIII], is a good match to the observed [OIII]/Hβ ratios for LINERs shown in Figure 2. However, [OIII]λ5007 is weaker in LINERs than [OII]λ3727 due to their lower ionization. For the SDSS spectra used here, with typical $S/N_{\mathrm{med}} \sim 22$ Å^{-1}, measurements of [OIII] are less reliable than those of [OII]. In the LINER-like galaxy sample, fewer than one third of all galaxies have [OIII] EW detections at or above a 3σ confidence level whereas more than 75% have $> 3\sigma$ detections in [OII]. Because the LINER-like galaxies lie on a narrow sequence in EW([OII])-EW(Hα) space (see Figure 1), [OII] can provide an estimate of Hα emission which is less dependent upon the Balmer line strengths of the stellar template fit used to measure emission lines in Yan et al. (2006). Having estimated the Hα EW from [OII], we can use a theoretically predicted Balmer decrement to derive the expected emission line strengths of Hβ, Hγ, and Hδ.

The existence of a tight roughly linear scaling relation between EW([OII]) and EW(Hα) suggests that both emission lines are produced by the same mechanism. The classification of quiescent vs. LINER-like galaxies was based in part on a S/N criterion that both emission lines be detected at a 2σ confidence level. It is reasonable to assume that galaxies exist with very faint emission that is undetected above the stellar continuum in the $S/N_{\rm med} \approx 22$ Å^{-1} SDSS spectra. These galaxies would most likely be intrinsically LINER-like galaxies with emission line equivalent widths approaching zero and would be classed by us in the quiescent sample. Using a linear least-squares fit of EW(Hα) as a function of EW([OII]) and forcing the fit to go through the origin, we find that EW(Hα) ≈ 0.197 EW([OII]). This fit is shown as the dashed line in Figures 1a-b. Using this fit, the measured EW([OII]) for each galaxy is converted into an estimated EW(Hα) and then into an estimated Hα flux, using the median spectral continuum level around Hα in each spectrum. The wavelength range used for computing the Hα continuum level is the same as Yan et al. (2006, Table 3).

The theoretically predicted Balmer decrement Hα/Hβ for LINER- and AGN-like emission line ratios is 3.1 (Osterbrock & Ferland 2005), with further decrements Hγ/Hβ = 0.46 and Hδ/Hβ = 0.26 for the higher order Balmer lines. These values are fairly independent of the exact excitation mechanism. However, if there is dust within the galaxy in or around the emission line region, Hβ, Hγ and Hδ emission will be dimmed with respect to Hα. The Balmer decrement actually measured for LINER-like galaxies in the Yan et al. (2006) sample is Hα/Hβ = 4.1 ± 0.3, corresponding to reddening with $\tau = 0.28$ between Hα and Hβ, or $E(B-V) = 0.47$.

As already noted, the Balmer emission measurements in the Yan et al. analysis are highly dependent on the choice of stellar template, and Balmer line emission is weak in LINER-like objects; Hβ is detected at the 3σ level in less than 23% of the galaxies in the LINER-like sample. In light of this, we also examined the sample of bright galaxies with $B_T \leq 12.5$ mag compiled by Ho, Filippenko, & Sargent a decade ago. (Ho, Filippenko, & Sargent 1995, Ho, Filippenko, & Sargent 1997 and other papers in the series). In Ho, Filippenko, & Sargent (1997), they classify emission line galaxies based upon their emission line ratios (specifically log([OIII]λ5007/Hβ), log([NII]λ6583/Hα), and log([OI]λ6300/Hα)) as Seyfert, LINER, HII, or Transition Objects. For all objects in their catalog which are classified as LINERs and which satisfy our color cut, the median Hα/Hβ Balmer decrement is 3.27, only slightly higher than that predicted by theory. This suggests that there is very little dust absorption within these systems, corresponding to a reddening of $\tau = 0.053$ between Hα and Hβ, equivalent to $E(B-V) \approx 0.050$. The distribution of Hα/Hβ in their sample of LINERs is independent of galaxy luminosity and emission line strength. However, their spectra cover the nuclear region (the central ~ 200 pc) only, and therefore may not be an appropriate counterpart to the SDSS fiber spectra used in our analysis, which typically cover 0.35–1.1 galaxy effective radii corresponding to several kpc.

In view of the uncertainty in the value of the proper Balmer decrement, the analysis below was repeated for both Hα/Hβ = 3.27 (as in Ho, Filippenko, & Sargent 1997) and Hα/Hβ = 4.1 (as in Yan et al. 2006). To obtain an emission infill correction for Hγ and Hδ, we assumed intrinsic Balmer decrements of Hγ/Hβ = 0.46 and Hδ/Hβ = 0.26, with a reddening law that scales as $\tau \propto \lambda^{-0.7}$ (following Kauffmann et al. 2003 and Cardiel et al. 1998). In §4.1 we will show that the choice of Balmer decrement affects the stellar population ages measured from the Balmer lines, particularly in Hβ. The higher order Balmer lines (and Hδ in particular) are less affected, and the evidence is strong that while uncertainties in the Balmer decrement introduce uncertainties into our age measurements, they do not qualitatively change our main results.

2.3. *Composite Spectra*

Detailed SSP modeling requires high S/N spectra, ideally $S/N \geq 100$ Å^{-1}. Individual SDSS spectra in this sample typically have $S/N_{\rm med} \sim 22$ Å^{-1}, making it necessary to stack dozens of similar spectra to achieve adequate S/N for SSP modeling. In this paper, we explore the dependence of stellar population age, [Fe/H], and abundance ratios on aperture-corrected galaxy velocity dispersion[4](σ), and the observed LINER-like emission line strength as measured by the strength of the [OII]λ3727 emission line. To do this, we divide the LINER-like galaxy sample into six bins in σ, with σ = 70–120 km s^{-1}, σ = 120–145 km s^{-1}, σ = 145–165 km s^{-1}, σ = 165–190 km s^{-1}, σ = 190–220 km s^{-1}, and σ = 220–300 km s^{-1}. Bins in σ are chosen to contain roughly equal numbers of galaxies. Within each σ-bin, the LINER-like galaxies are further divided into bins of weak (EW([OII]) < 5 Å) and strong (EW([OII]) > 5 Å) emission strength. Each bin contains over 100 galaxies and has a $S/N_{med} \geq 230$ Å^{-1}. In total, there are 2141 galaxies with weak emission and 1775 with strong emission.

Once the LINER-like galaxies have been divided into weak and strong subsamples, there are almost five times the number of quiescent galaxies as there are either weak or strong LINER-like galaxies. For comparison with the weak and strong LINER-like galaxies, we construct a sample of 2000 quiescent galaxies. Figure 3 shows the distribution of EW([OII]) for the 10,284 in the quiescent sample as the open histogram along with a gaussian fit to the distribution. The distribution peaks ~ 0.3 Å below zero. This may mean that the zeropoint correction determined in Yan et al. (2006) is uncertain at this level. For LINER-like emission with EW([OII]) $\sim 5\times$ EW(Hα) and Hα/Hβ ~ 3, this produces ΔH$\beta \sim 0.02$ Å. An uncertainty at this level is insignificant in the stellar population modeling process, thus we ignore the possible small discrepancy in zeropoint.

To create a comparison sample of quiescent galaxies, we construct a gaussian distribution centered about EW([OII]) = 0 Å with $\sigma_{\rm [OII]} = 1.56$ Å to match the width of the distribution in Figure 3. This distribution is truncated at $\pm 2\sigma_{\rm [OII]}$ in order to exclude outliers which may contain low-level undetected emission. From this truncated gaussian, we randomly select 2000 galaxies for our analysis. The EW([OII]) distribution of the final quiescent sample is shown as the shaded histogram in Figure 3.

---

[4] Following Bernardi et al. (2003a) and Jørgensen, Franx, & Kjærgaard (1995), velocity dispersions are aperture corrected to a standard one-eighth of the effective radius using $\sigma = \sigma_{\rm fib}(r_{\rm fib}/\frac{1}{8}r_o)^{0.04}$, where $\sigma_{\rm fib}$ is the velocity dispersion measured in the fiber spectrum, r_o is the circular galaxy radius in arc seconds and $r_{\rm fib}$ is the spectral fiber radius, 1.5″ for SDSS. This correction is small, of order ∼6%.

The 2000 quiescent galaxies are then divided into six bins in σ as were the weak and strong LINER-like galaxies. The sample therefore includes 18 bins in total: six bins in σ by three bins in emission line strength, labelled as "quiescent", "weak", and "strong". The parameters of the various galaxy bins are summarized in Table 1.

In each individual spectrum, absorption lines are broadened by the internal velocity dispersion of the stars in the galaxy, which has the effect of reducing the depths of the lines in the higher-σ galaxies. To make a consistent comparison between separate bins in σ, all the spectra are smoothed to an effective $\sigma = 300$ km s^{-1} to match the highest-σ galaxies in the sample.[5] The spectra are coadded within each bin, using an algorithm which averages the unsmoothed spectra within small sub-bins in $\sigma_{\rm fib}$ before smoothing to $\sigma = 300$ km s^{-1} and coadding the sub-bins. This minimizes the effect of far outlier pixels by averaging out noise spikes in a single pixel before smoothing the spectra. The regions around bright skylines at 5577Å, 6300Å, and 6363Å (observed frame) are masked in the individual galaxies to produce clean stacked spectra. In addition to an average spectrum, the total S/N at each resolution element is computed to produce an error spectrum for each stacked spectrum.

It is possible, even likely, that the quiescent galaxy bins in fact contain galaxies which do have faint emission lines but the galaxy spectra are too low S/N for the emission lines to be detected at the $> 2\sigma$ level that would qualify them for the LINER-like classification. We have attempted to remove some of these cases by truncating the EW([OII]) distribution at $\pm 2\sigma_{\rm [OII]}$, as described above. If a substantial number of weak emission line objects remain, these could produce non-negligible emission infill in the stacked spectra of quiescent galaxies. A check against this is to measure the [OII] emission in the stacked quiescent galaxy spectra, which have extremely high S/N. This is done in the same way as for the individual spectra, subtrating off a stellar absorption line template before making an emission line measurement, using the procedure described in the appendix of Yan et al. (2006). The EW([OII]) values measured for the quiescent stacked spectra are -0.01 Å, 0.04 Å, 0.41 Å, -0.27 Å, 0.28 Å, and -0.44 Å for the $\sigma = 70$–120 km s^{-1}, 120–145 km s^{-1}, 145–165 km s^{-1}, 165–190 km s^{-1}, 190–220 km s^{-1}, and 220–300 km s^{-1} stacked spectra, respectively. The largest of these [OII] EWs, 0.41 Å, corresponds to an Hα EW of 0.082 Å and an Hβ EW of 0.027 Å, using the scaling of equation 2 and the theoretical Balmer decrement. This level of contamination in Hβ is within the measurement errors of the Hβ Lick index for these high S/N spectra (see §3.1).

The stacked spectra with 70 km s^{-1} $< \sigma <$ 120 km s^{-1} are shown in Figure 4 as examples of the quality and resolution of the stacked spectra. The black line shows the quiescent galaxy bin, the green line shows the galaxies with weak LINER-like emission, and the red line shows the galaxies with strong LINER-like emission. The weak and strong LINER-like bins have been corrected for emission infill. The weak and strong bins *without* the emission infill correction are over plotted as dotted lines; the only differences appear in the Balmer absorption lines where the emission infill correction has been made. Prominant emission features are indicated by vertical dashed lines and are labelled. Other than the emission features, the spectra are remarkably similar, which shows both the high S/N of the stacked data and the subtleness of the spectral differences that are studied in this paper.

2.4. *Sample Completeness*

The galaxy sample presented here is a magnitude-limited sample, as described in §2.1, chosen within a narrow range in redshift ($0.06 < z < 0.08$). The galaxy bins, however, are defined in terms of σ. This means that the galaxy bins will be incomplete at faint magnitudes, where galaxies of a given σ may exist but be too faint to make it into the sample. Because galaxy magnitude and velocity dispersion are related through the Faber-Jackson relation (Faber & Jackson 1976), the lowest-σ bins will be most affected by this incompleteness. If the stellar populations of fainter galaxies differ systematically from those of brighter galaxies at the same σ, the results obtained from the stacked spectra will be biased at low σ. There is every reason to expect that the stellar populations will indeed differ, since fainter magnitudes at the same σ likely imply larger mass-to-light ratios. The incomplete low-σ bins will be biased toward brighter, and therefore possibly younger and/or more metal-poor stellar populations.

The top panel of Figure 5 shows a color-magnitude diagram (CMD) of the quiescent and LINER-like galaxy samples. Galaxies have been selected by the color cut described in §2.1, so only red sequence galaxies are included (compare to Figure 1c). The data points are color-coded by σ as explained in the caption. The dashed line at ${}^{0.1}M_r = -19.89$ shows the completeness limit at $z = 0.08$. The solid line at ${}^{0.1}M_r = -19.63$ shows the magnitude at which the sample is incomplete at the 50% level (i.e. missing half the galaxies at that magnitude). Thus the dashed line shows where the sample begins to miss galaxies and the solid line shows a point at which the sample has become severely incomplete.

In the lower panels of Figure 5, CMDs for each of the six ranges in σ are shown separately. In each CMD, the gray points show the entire sample of quiescent and LINER-like galaxies. Overplotted are colored contours showing the distribution of galaxies within a given range of σ. Solid and dashed lines indicate the 50% and 100% completeness limits respectively, as in the top panel. Below each CMD is a histogram of the ${}^{0.1}M_r$ values for the galaxies in each σ range.

Two well-known trends are immediately visible: higher σ galaxies are brighter (Faber-Jackson), and higher σ galaxies are redder, producing the slope of the red sequence. What is worthy of note is that at fixed σ, there is little if any slope to the color-magnitude relation. This is consistent with the claim of Bernardi et al. (2005) that the color-magnitude relation is purely a result of color-σ and magnitude-σ relations which are more fundamental, and Figure 5 gives a straight-forward visual confirmation of their result.

By comparing the distribution of the galaxies in each σ range (both the 2-dimensional distribution in the CMD as shown in the contour plots, and the 1-dimensional histogram in ${}^{0.1}M_r$), we can determine the level of incompleteness in each σ range. The lowest-σ range, shown in purple, is significantly incomplete; the distribution of ${}^{0.1}M_r$ has not even reached a peak at the completeness limit (dashed line) and the turn-over in the histogram may be entirely due to incompleteness. In this σ range, the stacked spectra will be missing the contribution of the faintest galaxies and will thus give an estimate of mean stellar population properties which is biased toward brighter galaxies at fixed σ.

---

[5] Note: Galaxies are binned by aperture-corrected σ, as this is the best estimate of an *intrinsic* property of the galaxy. For the purpose of measuring absorption line indices, all galaxies are smoothed based on their *observed* $\sigma_{\rm fib}$ to simulate the effect of uniformly observing all galaxies with broadening of 300 km s^{-1}.

To estimate the incompleteness of each σ range, we assume that the highest σ range ($\sigma = 220$–300 km s^{-1}) is complete and that its distribution in ${}^{0.1}M_r$ represents the true distribution in ${}^{0.1}M_r$ for each range. The histogram of ${}^{0.1}M_r$ for this range (shown in red in the lower right corner of Figure 5) shows an extended tail to fainter magnitudes. This tail is also visible in the $\sigma = 190$–200 km s^{-1} range and is suggested in the $\sigma = 165$–190 km s^{-1} range, thus lending support to the assumption of similar ${}^{0.1}M_r$ distributions in all σ ranges. In each σ range, the complete (bright) end of the normalized ${}^{0.1}M_r$ distribution is fit to the normalized $\sigma = 220$–300 km s^{-1} distribution and the discrepancy between the current range and the $\sigma = 220$–300 km s^{-1} range at the faint end is used to estimate the fractional incompleteness of the lower σ range. We find that the missing galaxies constitute approximately 51%, 28%, 19%, 11%, and 4% of the $\sigma = 70$–120, 120–145, 145–165, 165–190, and 190–220 km s^{-1} ranges, respectively. The estimated fractional incompleteness for each σ range is shown in Table 1.

This indicates that the lower σ ranges are significantly incomplete. If there are systematic differences between the stellar populations of bright and faint galaxies at fixed σ, the average stellar population parameters derived from the stacked spectra of *decreasing* σ ranges will be *increasingly* biased toward the bright galaxies at fixed σ. In appendix A we show that in fact the fainter galaxies at fixed σ have systematically weaker metal absorption lines than the bright galaxies, but that their Balmer absorption lines are the same. This suggests that the fainter galaxies are more metal poor and somewhat older than the brighter galaxies at fixed σ. We will correct for the effect of this trend in our incomplete data in §3.1.

3. LICK INDEX LINE STRENGTHS

3.1. *Line Strength Measurements*

In each stacked spectrum, we measure absorption line strengths of the Lick indices, as defined in Worthey et al. (1994) and Worthey & Ottaviani (1997). These include the Balmer lines Hβ, Hγ_F, and Hδ_F, as well as numerous “metal lines”: five lines dominated by iron absorption (Fe4383, Fe4531, Fe5270, Fe5335, and Fe5406), and lines which are sensitive to the abundances of other elements (Mg$_1$, Mg$_2$, Mg *b*, CN$_1$, CN$_2$, G4300, C$_2$4668, Ca4227, Ca4455, NaD, TiO$_1$, and TiO$_2$). The Lick indices are measured using the IDL code **Lick_EW**, part of the **EZ_Ages** code package described in Graves & Schiavon (in preparation). **Lick_EW** uses the error spectra described in §2.3 to compute the statistical errors in the index measurements due to the finite S/N of the stacked spectra. The error calculation is based on the formulae of Cardiel et al. (1998) as given in their equations (33) and (37). In addition to the Lick indices, the 4000 Å break has been measured using the narrow definition of D$_n$4000 given in Balogh et al. (1999), with errors calculated from Cardiel et al. (1998) equation (38). Lick index line strengths for each stacked spectrum are given in Tables 2–4.

Five Lick indices are excluded from this analysis. These include the wide Balmer indices Hγ_A and Hδ_A, which are designed to measure the broad Balmer wings of A stars and are not relevant for the analysis of old (> 1 Gyr) stellar populations. Also excluded are the reddest iron lines Fe5709 and Fe5782 because they are weaker features than the bluer iron lines and therefore represent noisier measurements. Finally, we exclude the iron line Fe5015 because it is strongly contaminated by [O III]λ5007 emission in the LINER-like galaxies.

In order to have a uniform sample, the stacked spectra are all smoothed to $\sigma = 300$ km s^{-1} to match the σ of the most massive galaxies (see §2.3). The combined resolution of $\sigma = 300$ km s^{-1} and the native SDSS resolution is at *lower* resolution than the Lick/IDS instrument resolution at which the Lick indices are defined. The index measurements must therefore be corrected back to effective Lick/IDS resolution. This correction is performed by **Lick_EW** using velocity dispersion corrections determined from smoothed SSP spectra from Schiavon (2007, Table A2a). The indices reported here are therefore effectively at Lick/IDS resolution. However, no zeropoint correction is performed to place them on the original Lick/IDS system. This is for two reasons. Firstly, the Lick standard stars are not observed by the SDSS—they are too bright—thus the data needed to make this correction do not exist. More importantly, the SSP models which we use to interpret the index measurements in §4.1 are defined using flux-calibrated spectra and are themselves not zeropoint-shifted to the Lick/IDS system. Because the SDSS spectra are also flux-calibrated, any zeropoint offset between the indices measured in SDSS spectra and the models should be small (see discussion in Schiavon 2007).

Figure 6 shows the indices measured in the stacked spectra as a function of the mean σ in each bin. Colors correspond to the emission line properties of the galaxies as follows: quiescent galaxy bins are shown in black, those with weak LINER-like emission in green, and those with strong LINER-like emission in red. In each of the panels a–d, the left column shows the Lick index line strengths measured in the stacked spectra. The error bars include statistical errors due to finite S/N only—no systematic errors are included. The lines show least squares fits of index strength onto σ for each bin in emission line strength.

In §2.4, we demonstrated that the lower σ bins are significantly incomplete at faint magnitudes. A correction for this effect, described in detail in Appendix A, is applied to the measured Lick index line strengths; these corrected line strengths are shown in the right columns of panels a–d in Figure 6. For the moment, we note merely that the correction is a small effect in all indices and has no qualitative effect on the following discussion.

No attempt has been made to correct the line strengths for variations in aperture. The range of redshifts in this sample spans a factor of 30% in angular diameter distance, but because the redshift distributions of quiescent, weak, and strong LINER-like galaxies are similar, the differences in mean physical aperture radius between the samples under comparison are negligible.

3.2. *Line Strength Trends with σ and Emission Properties*

In SSP models with ages over 1 Gyr, Balmer line strengths *decrease* with increasing SSP age. In the same models, the 4000 Å break (D_n4000), the CH band (G4300), and all of the metal line strengths *increase* with increasing SSP age (Worthey et al. 1994, Worthey & Ottaviani 1997, Bruzual & Charlot 2003, Thomas, Maraston, & Bender 2003, Schiavon 2007). However, line strengths are also affected by the metallicity of the SSP. In the same models, increasing the metallicity changes the line strengths in the same direction as increasing the SSP age: Balmer line strengths *decrease* while D_n4000, G4300, and metal line strengths *increase* with increasing SSP metallicity. These effects are summarized in Table 5 for those unfamiliar with SSP model results.

Figure 6a shows the Balmer lines Hβ, Hγ_F, and Hδ_F, as well as D_n4000 and G4300. All of these indices vary systematically with σ such that, as σ increases, the Balmer lines get weaker and D_n4000 and G4300 get stronger. Panels b–d in Figure 6 show line strengths for the metal lines. These indices show the same trends as D_n4000, and G4300: composite galaxy spectra with higher σ have *stronger* metal absorption lines than those with low σ. The stellar populations of the galaxies presented here vary systematically with σ, as has been seen previously by many authors.

It is also clear from Figure 6 that, at fixed σ, galaxies with strong LINER-like emission (red points) typically have stronger Balmer line absorption and weaker D_n4000, G4300, and metal lines than galaxies with weak LINER-like emission (green), which in turn have stronger Balmer lines and weaker D_n4000, G4300, and metal lines than the quiescent galaxies (black). This suggests that, in addition to a relationship between the stellar populations and σ, stellar populations also vary with the emission line strength of the galaxy. This trend exists not only in the Balmer lines, which are sensitive to errors in the emission infill correction made in §2.2, but also in D_n4000, G4300, and the metal lines which are not affected by contamination from either the emission or the chosen emission infill correction.

The sodium line NaD is the one exception to the trend that metal lines weaken as LINER-like emission strength increases; NaD absorption strengths *increase* with increasing LINER-like emission and typically vary by several tenths of an Å between quiescent and strong emission galaxies at fixed σ. NaD is a resonance line and is known to be significantly affected by interstellar absorption. In their sample of Galactic globular clusters, Gorgas et al. (1993) assume that up to 0.8 Å of the observed NaD line strengths is due to interstellar rather than stellar absorption. If the intrinsic *stellar* NaD line strength in galaxies actually follows the behavior of all the other metal lines and *decreases* with increasing emission, then the observed *increase* of NaD absorption with emission suggests that LINER-like galaxies contain more cold interstellar material than their quiescent counterparts, which serves to enhance the observed NaD absorption. This is discussed in greater detail in §5.1.

The trends visible in Figure 6 (with the exception of NaD, as discussed above) are consistent with the hypothesis that stars in galaxies with higher σ are typically *older* than those in lower-σ galaxies, and that at fixed σ galaxies with LINER-like emission have *younger* stars on average than their quiescent counterparts. However, as shown in Table 5, increasing SSP age changes all index strengths in the same direction as increasing SSP metallicity. This means that the observed trends with σ and emission strength may be trends in age, trends in metallicity, or some combination of the two. Fortunately, although the response of the various lines to changes in age is qualitatively similar to the response to changes in metallicity, there are quantitative differences: the Balmer lines are more sensitive to changes in age and less sensitive to changes in metallicity than are the metal lines. By comparing SSP model predictions to pairs of measured line strengths that differ quantitatively in their sensitivity to age and metallicity, we can break the "age-metallicity degeneracy." This is done in §4.1.

3.3. *Effect of the Infill Correction on Balmer Line Strengths*

Figure 6 shows that galaxies with LINER-like emission typically have stronger Balmer absorption lines than quiescent galaxies at the same σ. However, the strength of this effect depends critically upon the assumptions made in §2.2 in correcting for emission infill in these galaxies. It is instructive to examine the total effect of the emission infill corrections to understand their significance for Balmer absorption line strengths.

Figure 7a-c plots the Balmer lines as measured in the composite spectra without any emission infill correction. As in Figure 6, black, green, and red data points show quiescent, weak, and strong LINER-like emission galaxy bins, respectively. The emission infill is a large effect in Hβ, showing significant infill from emission in both weak and strong LINER-like galaxies. However, the infill in Hγ_F is substantially less, and is least significant in Hδ_F due to the Balmer decrement. Even without any emission infill correction at all, Hδ_F still shows a trend of stronger Balmer absorption in stronger LINER-like galaxies. Moreover, making no infill correction at all is obviously wrong, as can be seen by the substantial infill in the uncorrected Hβ. Any infill correction will only make the trend in Hδ_F stronger.

Figures 7d-f and 7g-i show the Balmer lines measured with the two different assumptions for the Balmer decrement that were described in §2.2: Hα/Hβ = 4.1, as measured by Yan et al. (2006), and Hα/Hβ = 3.27, as seen in the Ho, Filippenko, & Sargent (1997) red sequence LINERs. The choice of Balmer decrement makes some difference in the Hβ measurement (as can be seen comparing Figure 7f and 7i), but it is a small effect for Hγ_F (Figure 7e and 7h) and is practically negligible for Hδ_F (Figure 7d and 7g).

The infill correction Hα/Hβ = 4.1 gives Hβ absorption line strength values that cross at high σ; at $\sigma < 190$ km s^{-1} galaxies with LINER-like emission have stronger Hβ absorption than their quiescent counterparts, but above $\sigma = 220$ km s^{-1}, the Hβ absorption in the LINER-like galaxies is weaker than in the quiescent galaxies. In §4.1 we will show that this results in age trends that reverse for galaxies with $\sigma < 190$ (where LINER-like galaxies are younger than the quiescent galaxies) versus those with $\sigma > 220$ (where LINER-like galaxies are older than the quiescent galaxies). It is difficult to find a physical justification for this reversal of the trend in Hβ (and therefore age) with emission strength, and furthermore this reversal is not corroborated by Hγ_F or Hδ_F; the simpler explanation is that assuming a Balmer decrement of Hα/Hβ = 4.1 *underestimates* the appropriate emission infill correction. Figure 7f shows that the reversal described here is hardly a significant effect but would be larger for even larger values of the Balmer decrement; therefore this argument suggests that Hα/Hβ = 4.1 is an upper limit on the Balmer decrement.

Using Hα/Hβ = 3.27 gives consistent trends with LINER-like emission strength versus σ for all Balmer lines, with Hβ line strengths that converge to a single value for all emission strengths at high σ. If the intrinsic Balmer decrement for these LINER-like galaxies is similar to that of AGN (which have Hα/Hβ = 3.1, Osterbrock & Ferland 2005), then this is very close to the theoretical (unreddened) lower limit on the Balmer decrement. It is therefore likely that these two values enclose the true mean value, and $3.27 <$ Hα/Hβ < 4.1 for these systems.

The assumption that LINER-like emission is similar to AGN emission is not necessarily a legitimate one. Emission from stellar-ionized HII regions has Hα/Hβ = 2.86 in the absence of dust absorption (Osterbrock & Ferland 2005). For the sake of completeness, Figure 7 also shows the Balmer lines with an infill correction assuming this theoretical HII region value. The strength of Hβ changes noticeably, but the effect on Hδ_F is within the measurement errors. In summary, Hα/Hβ = 3.27 appears to be a reasonable value for the mean reddened Balmer decrement and it is almost certain that $2.86 <$ Hα/Hβ < 4.1. From Figure 7, it is clear that the exact value of the mean Hα/Hβ has some effect on Hβ line strengths but does not qualitatively changing the trends described in §3.2 above, and that Hγ_F and Hδ_F are only marginally affected by the exact value of the decrement.

4. STELLAR POPULATION MODELING: PROCEDURES AND CAVEATS

4.1. *SSP Models*

Stellar population models make it possible to convert measured index strengths into fundamental stellar population parameters (i.e., age, [Fe/H], and elemental abundance ratios). In this paper, we have chosen to use the models of Schiavon (2006; hereafter S06), which are based on fitting functions. Although the models produce SSPs rather than more complicated star formation histories, they include the effects of multiple individual elemental abundances in addition to mean age and [Fe/H].

The S06 models calculate predicted Lick index values for a model SSP with a specified abundance pattern. Non-solar abundance patterns change the SSP model through two different channels. The first is the effect on the isochrone of a non-solar abundance pattern, which changes the temperature and luminosity of the main sequence turn-off and red giant branch. The S06 models incorporate this effect (although in a limited way) by providing the option to construct the SSP model based on one of two isochrones: the solar-scaled isochrone of Girardi et al. (2000) or an α-enhanced isochrone from Salasnich et al. (2000) with average [α/Fe] = +0.42.[6] The second way in which non-solar abundances enter the SSP models is through their effect on the various line opacities of stellar atmospheres. In modeling line opacities, the S06 models take into account the effects of the elements C, N, O, Mg, Ca, Na, Si, Cr, and Ti. Stellar line opacities due to various elements and molecules may lie within the index passband of a Lick index, enhancing the strength of the measured index. They may also lie in the blue and red continuum regions on either side of the index against with the index absorption strength is measured. In this latter case, increased absorption *weakens* the measured Lick index strength. The Korn, Maraston, & Thomas (2005) index response functions are used to calculate the effect on the model Lick indices due to each of the elements listed above.

It should be emphasized that the S06 models are computed *at fixed [Fe/H]*, rather than at fixed total metallicity ([Z/H]), as is the case in many other stellar population models. This has several benefits. The first is one of simplicity and conceptual transparency. For models computed at fixed [Z/H], changing the α-enhancement of the model also changes [Fe/H]. Total metallicity is in fact dominated by oxygen (an α-element), so that changing [α/Fe] a small amount results in a large change in [Fe/H] in order to keep [Z/H] constant. It is therefore conceptually more complicated to keep track of how enhancing [α/Fe] affects stellar populations because one must disentangle the effects of increasing α-elements from the effects of decreasing [Fe/H]. One case where this is particularly important is that of the higher order Balmer lines, which are strongly affected by Fe I absorption lines in their continuum (Thomas, Maraston, & Korn 2004). In fixed [Z/H] models, changing [α/Fe] dramatically changes [Fe/H], which in turn has a strong effect on Hγ_F and Hδ_F. Because the S06 models are computed at fixed [Fe/H], the model predictions for Hγ_F and Hδ_F are relatively insensitive to [α/Fe]. This is discussed in detail in §5.2.

A second benefit of computing models at fixed [Fe/H] rather than fixed [Z/H] is that oxygen, which dominates total metallicity, is notoriously difficult to measure in the integrated light of stellar populations. While [O/H] remains essentially unmeasured, it is safer not to claim knowledge of total [Z/H]. This will be discussed in more detail in §4.3 and §5.3. A related point is that [Fe/H] is a parameter that is more directly related to measurable quantities (i.e., iron absorption lines such as Fe5270 or Fe5335) than is [Z/H], which depends on the abundances of many different elements. Some of these elements are not measured by any stellar absorption line, including the dominant element oxygen.

The S06 models take as input a set of abundance ratios and calculate Lick index values for the given abundances at a range of ages and [Fe/H]. The model produces grids of Lick index values for ages between 1.2 and 17.7 Gyr, and $-1.3 <$[Fe/H]$< +0.2$ for the solar-scale isochrone and $-0.8 <$[Fe/H]$< +0.3$ for the α-enhanced isochrone.

---

[6] The Salasnich et al. (2000) α-enhanced isochrone was computed using the following abundances: [O/Fe] = +0.50, [Ne/Fe] = +0.29, [Mg/Fe] = +0.40, [Si/Fe] = +0.30, [S/Fe] = +0.33, [Ca/Fe] = +0.50, [Ti/Fe] = +0.63, [Ni/Fe] = +0.02. All other abundances are solar.

The model grids can be used with index-index plots in the style pioneered by Worthey et al. (1994) to determine the age and [Fe/H] of an observed stellar population. Because the various Lick indices have different sensitivities to each elemental abundance, a best-fitting set of abundances can be found by tweaking the input abundances in the S06 models until all of the index-index plots give consistent values for the age and [Fe/H] of the stellar population in question.

The S06 models are limited to a subset of the Lick indices due to the restricted wavelength coverage of the stellar spectra used to construct the fitting functions. Only the Balmer indices (Hβ, along with both the broad and narrow Hγ and Hδ indices), Fe4383, Fe5015, Fe5270, Fe5335, Mg_2, Mg b, G4300, $\mathrm{C}_2$4668, CN_1, CN_2, and Ca4227 are modeled. This set of indices makes it possible to constrain the abundances [Mg/Fe], [C/Fe], [N/Fe], and [Ca/Fe], but [O/Fe], [Na/Fe], [Si/Fe], [Cr/Fe], and [Ti/Fe] are relatively unconstrained. In our analysis, we predominantly use the solar-scaled isochrone and set [O/Fe] to match the isochrone (i.e. [O/Fe] = 0.0). We also show results computed using the α-enhanced isochrone and with [O/Fe]=+0.3 for comparison. Because Na, Si, and Ti are α-elements, we force their abundances to follow [Mg/Fe], while the iron-peak element Cr tracks Fe ([Cr/Fe] = 0.0).

4.2. *Fitting for Ages and Abundances*

Fitting for the best set of input abundance ratios is done using the IDL code package **EZ_Ages** (Graves & Schiavon, in preparation). Briefly, **EZ_Ages** implements the method developed by Schiavon (2007) to determine abundances and ages of stellar populations. It uses an index-index plot of Hβ and $\langle\mathrm{Fe}\rangle$ (defined by $\langle\mathrm{Fe}\rangle = 0.5(\mathrm{Fe5270} + \mathrm{Fe5335})$) to measure a "fiducial" age and [Fe/H]. These indices are chosen because they are relatively insensitive to other, non-solar abundance ratios. **EZ_Ages** then uses an index-index plot of Hβ and Mg b to constrain [Mg/Fe]. This is done by varying [Mg/Fe] as input to the S06 model until the age and [Fe/H] measured in the Hβ-Mg b plot match the fiducial values from the Hβ-$\langle\mathrm{Fe}\rangle$ plot. In similar fashion, $\mathrm{C}_2$4668 is used to determine [C/Fe], CN_2 is used to determine [N/Fe] once [C/Fe] is set, and Ca4227 is used to get [Ca/Fe]. The entire process is then iterated in order to produce a self-consistent set of abundances. **EZ_Ages** then measures separately an age from Hγ_F and an age from Hδ_F using the best-fitting abundances. The result is a measurement of [Fe/H], [Mg/Fe], [C/Fe], [N/Fe], and [Ca/Fe], as well as ages measured from each of the three Balmer lines, for each set of measured Lick indices.

This abundance fitting must be done in a proscribed order. This takes into account the complicated effects of the various element abundances on the Lick indices used in the fitting procedure. The goal is to only introduce one new abundance ratio at a time. The Mg b index is sensitive to age, [Fe/H], and [Mg/Fe], but is relatively insensitive to all other abundance ratios (Korn, Maraston, & Thomas 2005, Serven, Worthey, & Briley 2005). Therefore, once the fiducial age and [Fe/H] have been determined, Mg b can be used to fit for [Mg/Fe]. The abundance ratios [C/Fe], [N/Fe], and [Ca/Fe] are more difficult to isolate. The [N/Fe] abundance ratio is difficult because its effect is seen most strongly in the CN_1 and CN_2 indices where [C/Fe] and [O/Fe] are also important factors; the Ca4227 index is highly sensitive to CN, as well as being sensitive to [Ca/Fe] because of a strong CN band in the blue continuum region around the index (described in detail in Prochaska, Rose, & Schiavon 2005); and [C/Fe] can best be isolated in the $\mathrm{C}_2$4668 index, however this index is also sensitive to [O/Fe] (Korn, Maraston, & Thomas 2005, Serven, Worthey, & Briley 2005). As mentioned above, oxygen is very difficult to measure in unresolved stellar populations.

In the **EZ_Ages** abudance fitting process, [C/Fe] is set first by fitting the $\mathrm{C}_2$4668 index, because $\mathrm{C}_2$4668 depends only on age, [Fe/H], [C/Fe], and [O/Fe]. Then CN_2 can be used to fit [N/Fe] because [C/Fe] is already determined. Only once [C/Fe] and [N/Fe] are determined can Ca4227 be used to fit for [Ca/Fe], in order to account for the strong dependence of Ca4227 on CN. The fact that [O/Fe] remains unknown contributes a significant uncertainty to all of these abundance determinations, but is unavoidable. When presenting abundance measurements for our data in §5.3, we will illustrate the effect of changing [O/Fe] by 0.3 dex. In practice, changing [O/Fe] by this amount appears to have no effect on [Fe/H] or [Mg/Fe], some effect on [C/Fe], a substantial effect on [N/Fe], and almost no effect on [Ca/Fe].

In order to illustrate the effect of elemental abundances on different line indices and our abundance-fitting process, we show in Figures 8 and 9 a set of index-index plots for all of the Lick indices included in the S06 model. In each plot, solid lines connect models at fixed [Fe/H], while the dotted lines connect models of constant age. The three data points are from the stacked spectra of quiescent galaxies with σ = 70–120 km s^{-1}, σ = 145–165 km s^{-1}, and σ = 220–300 km s^{-1} plotted as the triangle, star, and square, respectively. The index measurement errors are smaller than the size of the plotting symbols.

The model shown here is computed with the **EZ_Ages** output best-fitting abundances for the σ = 70–120 km s^{-1} stacked spectrum: [Mg/Fe] = 0.120, [C/Fe] = 0.100, [N/Fe] = -0.002, and [Ca/Fe] = 0.010, calculated with a solar-scale isochrone, with solar [O/Fe], with Na, Si, and Ti abundances set to equal [Mg/Fe], and with solar [Cr/Fe]. Figure 8 shows the Lick indices which are used by **EZ_Ages** in the abundance fitting. Note that the σ = 70–120 km s^{-1} data point (triangle) which was used in the abundance fitting falls in the same place with respect to the grid lines in each index-index plot. This is the essence of the abundance fitting process and signifies that a mutually self-consistent set of stellar population parameters and abundance ratios has been found.

A check on the robustness of the abundance results is to compare these index-index plots with those in Figure 9, which were *not* used in the abundance fitting process. The location of the σ = 70–120 km s^{-1} data point in each grid in Figure 9 is consistent with its position in the grids of Figure 8, except for the G4300 index which is too strong in the best-fitting model and Hγ_F which is too weak in the best-fitting model. A similar discrepancy in G4300 was noted in Schiavon (2007) in comparisons with Galactic clusters M67 and NGC 6528. Sánchez-Blázquez et al. (2006) also show anomalous behavior in the G4300 index with respect to $\mathrm{C}_2$4668 in their sample of early-type galaxies. The G4300 index in globular clusters appears to plateau for iron abundances with [Fe/H] ≥ -0.7; above this [Fe/H] the G band feature continues to increase with metallicity but absorption lines in the continuum against which the G4300 line strength is measured also increase in strength in such a way as to maintain relatively constant values of G4300 over a range of metallicity. The $C_2$4668 index is in a region of the spectrum where it is possible to define continua which are less affected by absorption. We thus consider $C_2$4668 to be a more reliable indicator of carbon enhancement than G4300. As for Hγ_F, we will show in §5.2 that Hγ_F and Hδ_F generally give *younger* age estimates than Hβ based on a SSP model and discuss the implications of this effect.

Unlike the σ = 70–120 km s^{-1} data, the σ = 145– 165 km s^{-1} and σ = 220–300 km s^{-1} data points (star and square) do not fall in the same location on each grid. The Mg, CN, and $C_2$4668 lines are particularly discrepant. This is because the grids were constructed to match the σ = 70–120 km s^{-1} data. In order to produce model grids that match these higher σ data points, [Mg/Fe], [C/Fe], and [N/Fe] must be increased (which shifts the model grids for the Mg, CN, and $C_2$4668 indices in Figures 8 and 9 to the right, toward the data). This suggests that higher σ galaxies have larger [Mg/Fe], [C/Fe], and [N/Fe]. In §5.3 we show that this is indeed in the case.

For comparison, Figures 10 and 11 show index-index plots computed with a different set of abundance ratios. Here we have used the best-fitting abundances for the $220 < \sigma < 300$ km s^{-1} data, which have [Mg/Fe] = 0.260, [C/Fe] = 0.270, [N/Fe] = 0.220, and [Ca/Fe] = 0.040. As before, the other α-elements (Na, Si, and Ti) follow Mg, while O and Cr have solar abundances. In Figure 10, the $220 < \sigma < 300$ km s^{-1} data (squares) give the same age and [Fe/H] values in each index-index plot. Because this model has enhanced [Mg/Fe], [C/Fe], and [N/Fe], the plots of Hβ against Mg *b*, $C_2$4668, and CN_2 are now consistent with the Hβ-$\langle$Fe$\rangle$ plot for the $220 < \sigma < 300$ km s^{-1} data. In contrast, the lower σ data points in these plots lie at values of [Fe/H] that are too low to match those from the Hβ-$\langle$Fe$\rangle$ plot. Figure 11 shows the indices that are not used in the abundance fitting. As before, the plots of Hβ against Fe4383, Mg_2, and CN_1 are consistent for the $220 < \sigma < 300$ km s^{-1} data, while the G4300 index produces ages that are too young. Here the ages measured from Hγ_F and Hδ_F are somewhat younger than those measured from Hβ.

An important caveat applies to the ages and abundances presented in the following sections. The S06 model fitting functions are constructed from flux-calibrated stellar spectra with no zeropoint correction to bring them onto the original Lick/IDS system. The SDSS spectra used in this analysis are also flux-calibrated, so zeropoint offsets between the model index system and the data should be small. However, as with most stellar population models based upon index measurements, *relative* values of stellar population parameters are more reliable than absolute measurements due to the zeropoint uncertainties.

4.3. *Oxygen Abundances in Old Stellar Populations*

It is unfortunate that it has not been possible thus far to measure oxygen abundances in unresolved stellar populations. Not only is oxygen the single most abundant metal in the Universe, but main sequence turn-off temperatures are substantially affected by oxygen abundances (Vandenberg & Bell 2001). An inability to determine the oxygen abundance therefore means that the total metallicity is unknown and the true isochrone shape is not well-known, raising uncertainties in stellar population analysis.

Theoretical models of nucleosynthesis predict that Mg and O both originate in Type II SNe (e.g. Wheeler, Sneden, & Truran 1989, Woosley & Weaver 1995) and should track one another closely, but there is some evidence that this is not always the case. In a survey of 27 Milky Way bulge giants, Fulbright, McWilliam, & Rich (2006) find that, although Mg appears to be enhanced at all [Fe/H], [O/Fe] declines with increasing [Fe/H] and is solar or mildly sub-solar at [Fe/H] ≥ 0.0. This indicates that, at least in some stellar populations, the assumption that O varies in lockstep with Mg is not valid. In addition, there is growing evidence from X-ray observations that the hot gas in elliptical galaxies has subsolar values of [O/Fe] (Humphrey & Buote 2006, Humphrey, Buote, & Canizares 2004 and references therein) and also subsolar [O/Mg] (Humphrey & Buote 2006), further undermining the assumption that Mg and O vary together.

In light of these uncertainties, we treat [O/Fe] as undetermined. The S06 SSP models are computed for fixed [Fe/H] rather than fixed [Z/H] so the uncertainty in total metallicity should not have a large effect on the results of the stellar population modeling. In the following sections, we present results based on both the solar abundance and α-enhanced isochrones available with **EZ_Ages**, and at each stage of the analysis illustrate the effect of changing the oxygen abundance by exploring a range of values for [O/Fe].

5. STELLAR POPULATION MODELING RESULTS: AGES AND ABUNDANCES

5.1. *SSP Ages as a Function of σ and Emission Line Strength*

The **EZ_Ages** code was used to estimate mean luminosity-weighted ages and abundances from Lick index measurements for each of the stacked spectra. Using the best-fitting abundance models, we obtained ages for each stacked spectrum, measured separately from the Hβ-$\langle$Fe$\rangle$, Hγ_F-$\langle$Fe$\rangle$, and Hδ_F-$\langle$Fe$\rangle$ grids. We shall hereafter refer to these separate age measurements as "Hβ ages", "Hγ_F ages", and "Hδ_F ages", with the understanding that these indicate the ages as measured from index-index plots using the named Balmer line. Figure 12 shows these age measurements as a function of the mean σ in each galaxy bin and emission line strength, for each of the stacked spectra. The left panel shows the measured ages when a Balmer decrement of Hα/Hβ = 3.27 is assumed, while the center panel assumes Hα/Hβ = 4.1. In both cases, the **EZ_Ages** fitting has been computed with a solar-scaled abundance isochrone. The right panel shows the effect of using the α-enhanced isochrone and [O/Fe] = +0.3 in the **EZ_Ages** fitting process. The Hβ ages, Hγ_F ages, and Hδ_F ages are plotted separately in each panel, from top to bottom. The error bars show the uncertainty in the ages due to measurement errors in the Balmer lines and $\langle$Fe$\rangle$ only. The solid lines are linear least squares fits of age onto σ.

The most striking result in this figure is that the galaxies with strong LINER-like emission are systematically *younger* than their quiescent counterparts at the same σ, with weak LINER-like galaxies falling in between. This trend exists in all of the age measurements, regardless of which Balmer line is used, and for either Balmer decrement. As expected from the line strength variations shown in Figure 7, the Hβ ages are most affected by the chosen decrement, while the Hδ_F ages are essentially unaffected. In §3.3, we argued that the two values of the Balmer decrement used here likely represent lower and upper boundaries for reasonable estimates of Hα/Hβ. Thus the panels of Figure 12 show the range of possible SSP age differences between quiescent and LINER-like galaxies. The use of an α-enhanced isochrone with [O/Fe] = +0.3 (right panel) results in Hβ ages that are consistently younger than those measured using a solar abundance isochrone but does not change the trend in age with emission strength.

The difference in measured age between quiescent and strongly emitting galaxies is substantial—ranging from around 3.5 Gyr in the lowest σ bin to 2 Gyr in the highest σ bin with Hα/Hβ = 3.27 and a solar-scaled isochrone, as measured in all Balmer lines. Galaxies with LINER-like emission contain stars which are on average 10–40% *younger* than those in quiescent galaxies of the same σ (using Hβ ages).

A second effect that is apparent in Figure 12 is that galaxies with high σ are on average *older* than those with low σ. This trend is apparent in ages measured by all Balmer lines, independent of the chosen Balmer decrement, and for quiescent as well as emission line galaxies (with the exception of Hδ_F ages in quiescent galaxies which are $\sim$ 7 Gyr, regardless of σ). This suggests that more massive galaxies formed a larger percentage of their stars in the distant past than did less massive galaxies, which seems to be consistent with the so-called "downsizing" phenomenon (Cowie et al. 1996, see also Bernardi et al. 2003b, Nelan et al. 2005, Thomas et al. 2005, Treu et al. 2005, and many others).

Interestingly, the Schiavon (2007) analysis of SDSS stacked spectra from Eisenstein et al. (2003) shows no increase in Hβ age with galaxy absolute magnitude but a definite increase in Hδ age, using the same models as in this work. That sample is selected predominantly by morphology and color, with no selection applied based on emission line properties. Because of this, the Eisenstein et al. (2003) sample likely contains not only quiescent and LINER-like galaxies, but a small contaminating fraction of galaxies with Seyfert and HII region emission as well. The emission infill correction applied by Schiavon (2007) is inaccurate for these galaxies, and appears to cause the discrepancy in the trends seen in Schiavon (2007) with the results presented here. Appendix B presents a detailed comparison between Schiavon (2007) and this work.

The stellar population modeling described above shows that the LINER-like galaxies have younger ages than their quiescent counterparts at fixed σ; it is natural to assume that they should therefore have slightly *bluer* colors. In fact, the opposite is true. As shown in Figure 13, the LINER-like galaxies typically have slightly *redder* colors than the quiescent galaxies at the same σ. The effect is small, ranging up to 0.037 mag in $^{0.1}(g\text{-}r)$ but is consistent across all galaxy bins. If the LINER-like galaxies are indeed younger than the quiescent galaxies at the same σ, they must also be subject to a larger degree of intrinsic interstellar reddening, on average. This hypothesis is corroborated by the observation that LINER-like galaxies appear to have stronger NaD absorption than their quiescent counterparts, suggesting that they are subject to a greater amount of internal interstellar absorption (see the discussion in §3.2).

More quantitatively, the younger ages measured for the LINER-like galaxies in the spectral line fitting (Figure 12) should make the LINER-like galaxies $\sim$ 0.06 mag *bluer* in $B-V$, based on the stellar population models of Bruzual & Charlot (2003). Instead, they are observed to be $\sim$ 0.04 mag *redder* in $B-V$.[7] This implies that the typical LINER-like galaxy is subject to internal reddening of $E(B-V) \approx 0.10$ beyond the (typically small) internal reddening of quiescent red sequence galaxies. This modest amount of reddening is reasonably consistent with the value $E(B-V) = 0.05$ that was used in our preferred computation of the Balmer decrement in §2.2, and is substantially smaller than the value $E(B-V) = 0.47$ that gives an upper boundary to reasonable values of Hα/Hβ above.

In the Milky Way, $E(B-V) = 0.10$ in the Galactic plane roughly corresponds to interstellar NaD absorption of $\sim$ 0.35 Å (Gorgas et al. 1993). This is generally consistent with the excess of NaD absorption in the LINER-like galaxies needed to bring the NaD stellar absorption strengths into line with the rest of the metal lines shown in Figure 6. The relation between $E(B-V)$ and NaD interstellar absorption observed in the Milky Way varies substantially outside the Galactic plane, making a calculation of $E(B-V)$ from observed NaD absorption necessarily inaccurate. However, it is clear that there is at least reasonable agreement between the internal reddening suggested by the median galaxy colors and the observed interstellar NaD absorption in the LINER-like galaxies. Thus, LINER-like galaxies typically suffer from a greater degree of internal reddening than their quiescent counterparts at fixed σ but this excess reddening is small, around $E(B-V) = 0.1$ on average.

5.2. *Ages Measured by Hγ_F and Hδ_F*

A third effect that is visible in Figure 12 is that ages measured with different Balmer lines vary systematically, such that bluer Balmer lines produce younger age measurements. This is true for the quiescent galaxies as well as the LINER-like galaxies, so it cannot be an artifact of the emission infill correction.

The Balmer lines Hγ_F and Hδ_F have been shown to be sensitive to non-solar abundance ratios in models computed at fixed [Z/H]. The effect of non-solar abundance ratios is strongest at high metallicity (Thomas, Maraston, & Korn 2004), and is thus particularly relevant for early type galaxies, whose metallicities are typically nearly solar or super-solar, unlike globular clusters, which are typically α-enhanced but are comparitively metal-poor. Thomas, Maraston, & Korn (2004) have demonstrated that, in models computed at fixed [Z/H], including the effects of α-enhancement raises the age estimates from $H\gamma_F$ and $H\delta_F$, and could thus in principal solve a discrepancy in which the bluer Balmer lines are producing younger age estimates than $H\beta$.

---

[7] The $^{0.1}(g-r)$ color has been converted to rest frame $B-V$ using Mike Blanton's *kcorrect* code, v. 3_2 (Blanton et al. 2003a) along with the empirical transformations from the SDSS *ugriz* magnitude system to Johnson B and V bands given by Jordi, Grebel, & Ammon (2006).

However, the sensitivity of $H\gamma_F$ and $H\delta_F$ is primarily a sensitivity to [Fe/H], rather than [α/Fe], and is an example of the complication of computing models at fixed [Z/H]. The abundance ratio dependence of $H\gamma_F$ and $H\delta_F$ is primarily due to the large number of iron absorption lines in the regions surrounding the $H\gamma_F$ and $H\delta_F$ indices (Thomas, Maraston, & Korn 2004). For models at fixed [Z/H], choosing a model with too low a value of [α/Fe] (i.e., a solar-scaled model when the galaxy is α-enhanced) means that the model has too *high* a value of [Fe/H] at fixed [Z/H]. This makes the Fe I absorption lines in the continuum regions on either side of the index passband too strong, lowering the continuum measurement and consequently lowering the measured value of the Balmer absorption index in the models. This makes the observed Balmer index look stronger in comparison to the models, and results in a *younger* age measurement. Using the correct [α/Fe] model fixes this problem, which has led Thomas, Maraston, & Korn (2004) to claim that α-enhancement effects cause younger ages to be measured in higher order Balmer absorption lines. However, the effect is dominated by Fe I lines. For models computed at fixed [Fe/H], the effect of the iron abundance on $H\gamma_F$ and $H\delta_F$ is accounted for, and does not depend on the α-enhancement of the model. Thus the claimed [α/Fe]-dependence of ages measured from $H\gamma_F$ and $H\delta_F$ is in fact a dependence on [Fe/H] that is translated into an α-enhancement effect in models at constant [Z/H]. The S06 models, which are computed at fixed [Fe/H] rather than fixed [Z/H] do not have this entangled dependency.

The S06 models produce consistent age measurements from $H\beta$, $H\gamma_F$, and $H\delta_F$ when they are used to analyze known SSPs such as the Galactic globular clusters 47 Tuc, M5, and NGC 6528, and the open cluster M67 (Schiavon 2007) which span a wide range of SSP parameters. Both 47 Tuc and M5 are metal-poor systems for which the α-enhancement effect on $H\gamma_F$ and $H\delta_F$ should be weak (Thomas, Maraston, & Korn 2004), and M67 is not significantly α-enhanced, thus these clusters are less relevant comparisons for high metallicity α-enhanced galaxies. However, NGC 6528 is relatively old, has roughly solar [Fe/H] and is mildly α-enhanced, with $age = 11 \pm 2$ Gyr, [Fe/H]$=$ 0.0 ± 0.15, [Mg/Fe]$=$ $+0.10 \pm 0.04$ and [O/Fe]$=$ $+0.1 \pm 0.05$ (Zoccali et al. 2004, Barbuy et al. 2004, Carretta et al. 2001, summarized in Table 10 of Schiavon 2007) and is thus an excellent SSP analog for early type galaxy data. The S06 best-fitting model for NGC 6528 has [Fe/H]$= -0.2$, [Mg/Fe]$= +0.1$, [O/Fe]$= +0.15$, and produces $H\beta$, $H\gamma_F$, and $H\delta_F$ ages of 13, 10, and 12 Gyr, respectively, which are relatively consistent within the uncertainties in the models.

In the red sequence galaxies analyzed in Schiavon (2007), however, the models produce age measurements that decrease as bluer Balmer lines are used. Schiavon (2007) has shown that the most likely explanation for this phenomenon is that galaxies are not SSPs but contain stars with a range of ages. This effect has also been reported by Sánchez-Blázquez et al. (2006); they also interpret the differing age measurements from different Balmer lines as due to extended star formation histories.

In Schiavon (2007), four possible explanations for this phenomenon are discussed: the presence of a subpopulation of young to intermediate-age stars, a significant number of blue stragglers, the presence of a metal-poor old stellar population with a blue horizontal branch, or the effects of strongly non-solar abundance ratios which are not constrained by the available Lick indices. Among these scenarios, Schiavon (2007) concludes that a young-to-intermediate subpopulation is the most likely; the blue horizontal branch scenario cannot reproduce all three Balmer lines simultaneously, the fraction of blue stragglers required to reproduce the observed line strengths is 10–100 times larger than blue straggler populations observed in Galactic globular clusters, and the abundance ratios that reproduce the observed line strengths seem extreme: [O/Fe] $= +1.0$, or [Ti/Fe] $= -0.7$.

In contrast, a small population of young-to-intermediate stars is sufficient to produce differences in Balmer line strengths similar to those observed. Schiavon (2007) shows that a 11.2 Gyr SSP combined with a superimposed young population with age $= 0.8$ Gyr and comprising 0.5–1.0% of the total stellar mass produces measured $H\beta$ age ~ 5 Gyr and $H\delta_F$ age ~ 3.5 Gyr. These ages correspond to the measured $H\beta$ and $H\delta_F$ ages of the $\sigma = 70$–120 km s^{-1} strong LINER-like emission stacked spectrum shown in Figure 12, with $H\alpha/H\beta = 3.27$, which can therefore be modeled as such a two-burst system. This simple example serves to illustrate that measurement and modeling of multiple Balmer lines in a single system has the potential to reveal extended star formation histories. More sophisticated analysis of these galaxy spectra using composite stellar populations is beyond the scope of this work but is clearly worthy of future investigation.

It is noteworthy that almost all of the stacked spectra in our sample—quiescent and LINER-like, low σ and high σ—display this discrepancy in ages as measured by different Balmer lines. The only exception is the lowest σ quiescent galaxy bin, for which $H\beta$, $H\gamma_F$, and $H\delta_F$ ages are relatively consistent at 8.4, 5.9, and 7.0 Gyr, respectively.

One could postulate that the younger ages in bluer Balmer lines, instead of indicating a composite stellar population, were in fact caused by an inadequate treatment of α-enhancement in the S06 models, although we have argued above that $H\gamma_F$ and $H\delta_F$ are strongly affected by α-enhancement only in stellar population models computed at fixed [Z/H]. A systematic variation of $H\gamma_F$ and $H\delta_F$ with [α/Fe] could produce the trend observed in the quiescent galaxies: that the higher σ galaxies (which have higher [Mg/Fe], as shown below in §5.3) show younger ages in $H\gamma_F$ and $H\delta_F$ than in $H\beta$, but that all ages are nearly consistent in the lowest σ galaxy bins which have nearly solar abundance ratios. However, it would be difficult to then explain the fact that the weak and strong LINER-like galaxies *do* show younger $H\gamma_F$ and $H\delta_F$ ages at all σ. In the next section, we will show that the weak and strong LINER-like galaxies have virtually identical abundance ratios to the quiescent galaxies at the same σ, thus it is difficult to invoke abundance ratio effects to fully explain the trends in Figure 12.

If we were to take the age trends in Figure 12 at face value, the implication is that for quiescent galaxies, those with large σ have a spread of stellar ages, while those a lower σ are relatively close to SSPs. This would be in disagreement with compelling work by Thomas et al. (2005) who find more extended star formation histories in lower σ early type galaxies than in higher σ galaxies. It would also disagree with recent evidence from star forming galaxies at redshift $z \sim 1$ that lower mass galaxies have more extended star formation episodes (Noeske et al. 2007). However, younger ages in Hγ_F and Hδ_F *are* seen in Figure 12 for the galaxy bins with LINER-like emission, at all σ. If the galaxies which have experienced relatively recent star formation episodes are predominantly found in the weak and strong LINER-like classes, the classification by emission line strength may have isolated the low σ galaxies whose star formation ceased long ago and who may therefore be more likely to resemble SSPs. It is not immediately clear, however, why this would not also be the case for more massive galaxies. A more detailed investigation of complex model star formation histories would be necessary to further interpret the trends seen in Figure 12, which we defer to future work.

Detailed analysis of the age differences between Balmer lines may in fact be pushing the data farther than is reasonable, given the uncertainties in the stellar population modeling process and the unknown contribution of oxygen. In addition, any conclusion that is strongly dependent on the $\sigma = 70$–120 km s^{-1} and $\sigma = 120$–145 km s^{-1} bins should be regarded with caution, as those bins are known to be substantially incomplete (see §2.4).

An important caveat that pertains to both this work and the Schiavon (2007) study is that each of these stacked spectra are composites of the spectra of several hundred galaxies. The differences in ages measured from various Balmer lines may therefore merely indicate that the galaxies included in each bin have a range of stellar population ages, rather than that each individual galaxy contains a composite stellar population.

5.3. *Abundances as a Function of* σ

Iron abundances and elemental abundance ratios measured with **EZ_Ages** are shown in Figure 14 as a function of σ. Plotted abundances are computed using a solar abundance isochrone with Hα/Hβ = 3.27; the abundances computed with Hα/Hβ = 4.1 or the α-enhanced isochrone (not shown) are very similar. As before, black, green, and red data points show results for quiescent, weak, and strong LINER-like galaxies respectively. The dotted line in each panel shows the solar value for reference. Error bars are 1σ errors computed in **EZ_Ages** by summing in quadrature the errors in each abundance due to individual Lick index measurement errors. The effect of errors in the fiducial ages and [Fe/H] are propagated through the abundance ratio estimates. Graves & Schiavon (in preparation) will discuss the error calculations in greater detail.

Unlike the mean, lightweighted SSP ages that were shown in Figure 12, the [Fe/H] and abundance ratios of the stacked galaxy spectra do not appear to vary with emission line strength; at fixed σ, quiescent and LINER-like galaxies appear to have the same average abundance pattern within the errors. This means that the metal absorption line variations with emission line strength that are apparent in Figure 6 are caused by variations in mean galaxy age, rather than by abundance differences.

The chemical abundances do however depend on σ. The solid black lines in Figure 14a–e are linear least squares fits of the abundances onto σ. A single line is used to fit quiescent, weak, and strong LINER-like galaxies simultaneously. For ease of comparison, the scale of the y-axis is the same in panels a–e. All abundances and abundance ratios increase with increasing σ such that high σ galaxies are both more metal-rich and more enhanced in light elements with respect to Fe than are the low σ galaxies.

[Fe/H] increases with increasing σ as [Fe/H] $\propto \sigma^{0.45}$, and is observed to range from about 1/2 solar at $\sigma \sim 100$ km s^{-1} to slightly sub-solar at $\sigma \sim 250$ km s^{-1}. Because early-type galaxies are known to have substantial metallicity gradients (Carollo, Danziger, & Buson 1993, Ogando et al. 2006), the zero-point of the [Fe/H] relation is dependent upon the aperture used to extract the spectral data. The SDSS 1.5″ spectral fibers typically cover 0.35–1.1 effective radii and thus sample a large fraction of the galaxy light. Nuclear spectra of early-type galaxies (e.g. those of Trager et al. 2000b and Thomas et al. 2005) should appear substantially more metal-rich due to the metallicity gradients of the galaxies.

The galaxies in this sample are Mg-enhanced at all σ, with the highest σ galaxies being the most enhanced ([Mg/Fe] $\propto \sigma^{0.36}$). Both [C/Fe] and [N/Fe] increase strongly with σ, from solar values in the low σ galaxies to substantial C and N enhancement at high σ. Finally, Ca appears to follow Fe in all galaxies. Table 7 gives the slope of the solid line fit for each elemental abundance or abundance ratio, along with the 1σ uncertainty in the slope.

The tendency of Ca to remain relatively constant with σ, rather than to follow Mg and other α-elements as expected if Ca production is dominated by Type II supernovae (Woosley & Weaver 1995), has been known for some time. It has been seen both in the Ca4227 index, which appears to be constant over a range of σ (e.g., Vazdekis et al. 1997, Thomas, Maraston, & Bender 2003) and in the near-IR Ca II triplet, which may even *anti*-correlate with σ (e.g., Saglia et al. 2002, Cenarro et al. 2003, and references therein). Recently, Prochaska, Rose, & Schiavon (2005) have demonstrated that the Ca4227 index is stronly affected by CN absorption in its blue continuum region and have suggested that redefining the Ca4227 index to avoid this region results in a Ca4227 index that is less sensitive to other element abundances. Unfortunately, the Korn, Maraston, & Thomas (2005) index sensitivities and the S06 models do not include the redefined Ca4227r index. In principal, the abundance fitting process described in §4.2, which fits for [C/Fe] and [N/Fe] before using Ca4227 to fit for [Ca/Fe], should account for the CN effect on Ca4227. Indeed, Schiavon (2007) uses the same abundance fitting method as in this paper and finds that [Ca/Fe] does increase with galaxy luminosity in a set of stacked SDSS spectra. However, the discrepancy between that result and our Figure 14 appears to be an artifact due to imperfect emission infill correction in the Hβ feature in the Schiavon (2007) analysis. Details of this are provided in appendix B.

An interesting result from this Figure is that [C/Fe] and [N/Fe] show the strongest variation with σ, with considerably steeper slopes than [Mg/Fe]. The value of [Mg/Fe] is measured here using the Mg *b* Lick index, and has been used in past works (e.g., Trager et al. 2000a) to trace the enhancement of α-elements ([α/Fe]). If Mg is indeed a good proxy for the bulk of the α-elements, the relative strength of the abundance-σ relations shows that [C/Fe] and [N/Fe] vary more strongly with σ than does [α/Fe].

It has been suggested in previous work that [C/Fe] and [N/Fe] are enhanced above solar ratios. Trager et al. (2000a) prefer a model for abundances in elliptical galaxies that has C and N enhanced along with the α-elements O, Ne, Na, Mg, Si, and S, but state that a similar model with solar C is difficult to distinguish from their preferred model based on the data. Sánchez-Blázquez et al. (2006) prefer an abundance model in which the α-elements Na, Si, Ca, O, and Ti are enhanced at higher σ, with C enhanced but as a less steep function of σ than the α-elements, with N enhanced more steeply than the α-elements, and with Mg enhanced most strongly of all. The results presented here differ from both Trager et al. (2000a) and Sánchez-Blázquez et al. (2006) in that we show [C/Fe] and [N/Fe] enhancement to increase *more strongly* with σ than does [Mg/Fe]. All of these results are at odds with the C enhancement pattern found by Clemens et al. (2006), who find that [C/H] *decreases* with increasing σ. It is clear that there is no consensus as to the enhancement (or depletion) pattern of these light elements.

One difference in the modeling process is that the models used in our analysis were computed at [O/Fe] = 0.0, whereas the other three works mentioned above have oxygen enhanced along with the α-elements. The dashed line in Figure 14a–e shows the effect of fixing [O/Fe] at +0.3 during the abundance fitting process instead of [O/Fe] = 0.0. Both [Fe/H] and [Mg/Fe] appear unchanged and [Ca/Fe] shows only a small difference, but [C/Fe] and [N/Fe] *increase* at all σ for the oxygen-enhanced models. This is because oxygen has a negative effect on the $C_2$4668 and CN index strengths used to compute [C/Fe] and [N/Fe]. In the presence of increased oxygen, most C will form CO rather than C_2 or CN, requiring larger C and N abundances in order to produce the observed C_2 and CN line strengths. Note that although there is a vertical offset, the slopes of the enhancement-σ relations do not change between the [O/Fe] = 0.0 and the [O/Fe] = +0.3 models. If [O/Fe] increases with σ following [Mg/Fe] as expected if both Mg and O production are dominated by Type II supernovae (SNe), it is clear that the high σ galaxies will be more enhanced above the [O/Fe] = 0.0 level than the low σ galaxies, causing the slopes of the [C/Fe]-σ and [N/Fe]-σ relations to be even steeper.

Many stellar population models are computed at fixed [Z/H], whereas the S06 models are computed at fixed [Fe/H]. To facilitate comparisons between models, Figure 14f shows [Z/H] as a function of σ, for five different assumptions about [O/Fe] values. [Z/H] was computed using the solar elemental abundances of Grevesse, Noels, & Sauval (1996). In calculating [Z/H], Cr, Mn, Fe, Co, Ni, Cu, and Zn are treated as Fe-peak elements and assumed to scale with the measured [Fe/H], while Ne, Na, Mg, Si, S, and Ti are treated as α-elements and assumed to scale with the measured [Mg/Fe]. C, N, and Ca are allowed to vary separately with their measured abundance ratios. All other elements are assumed to have solar abundances, excepting O. The black lines in Figure 14f show [Z/H] computed assuming constant O enhancement; [O/Fe] = 0.0, [O/Fe] = +0.3, and [O/Fe] = +0.5 are shown as the solid, dashed, and dash-dot black lines, respectively. The blue lines show [Z/H] computed with [O/Fe] that varies with σ. The solid blue line is computed assuming that O scales with the other α-elements ([O/Fe] = [Mg/Fe]), while the dashed blue line has O scaling with Mg, but enhanced by a factor of two above Mg ([O/Fe] = [Mg/Fe] + 0.3). The slopes of the relations are given in Table 7. Unsurprisingly, a steeper relation results when O scales with Mg because [O/Fe] increases with σ. Figure 14f highlights a problem with using models computed at fixed [Z/H]: total metallicity is dominated by O, which is highly uncertain and not measured.

As discussed in Appendix A, Figure 15 shows that, at fixed σ, galaxies with fainter magnitudes have weaker metal line strengths than brighter galaxies but almost identical Balmer line strengths, suggesting that fainter galaxies are more metal-poor than their brighter counterparts at the same σ. We have used the S06 models to convert the line strengths from Figure 15 into age and abundance estimates, following the same procedure described above for quiescent versus LINER-like galaxies. This modeling (not shown) confirms that fainter galaxies have lower values of [Fe/H] and older ages compared to brighter galaxies at the same σ, while their abundance ratios are nearly identical.

5.4. *Comparison with Previous Results*

To put the results presented here into the context of existing similar work, we have compiled results from four other SSP analyses of early type galaxies. Table 8 gives the slopes of the $\log age$–$\log\sigma$, [Fe/H]–$\log\sigma$, [Z/H]–$\log\sigma$, and [α/Fe]–$\log\sigma$ relations reported here and in previous work. Interestingly, although models claiming to accurately reproduce the effects of α-enhancement are relatively recent, the reported [α/Fe] values agree better than the ages or metallicities. There appears to be a consensus value of $d[\alpha/\mathrm{Fe}]/d\log\sigma = 0.32 \pm 0.04$.

All of the studies reviewed here find that typical galaxy ages increase with σ, although there is substantial variation in the reported values of $d\log age/d\log\sigma$, ranging from 0.24 (Thomas et al. 2005) to 1.15 (Bernardi et al. 2003b). Our value of $d\log age/d\log\sigma = 0.35$ is toward the shallower end of the reported trends. It is noteworthy that the age trends shown in Figure 12 for LINER-like galaxies are steeper than those for quiescent galaxies.

As for $d[\mathrm{Z/H}]/d\log\sigma$, our value of 0.79 ± 0.05 computed assuming [O/Fe]= 0.0 (see Table 8) is in excellent agreement with the Trager et al. (2000b) value of 0.76 ± 0.13, and is a little steeper than the trends reported by Thomas et al. (2005), Nelan et al. (2005), Smith, Lucey, & Hudson (2007), and Bernardi et al. (2003b). Because this work analyzes stacked spectra, we can only quantify mean trends and thus the age-metallicity hyperplane of Trager et al. (2000b) is not visible in this work.

6. DISCUSSION

We have shown that, on average, red sequence galaxies with LINER-like emission have *younger* SSP ages than quiescent galaxies at the same σ; strong LINER-like galaxies are 2–3.5 Gyr younger than their quiescent counterparts. This suggests that there is a connection between the star formation history of a galaxy and the presence or absence of LINER-like emission within it.

Several caveats apply to this statement. Most importantly, this study is based on stacked spectra, and therefore analyzes only the mean properties of galaxies in each bin of emission properties and σ. There may be a significant spread in the ages of galaxies within each bin; not all LINER-like galaxies are necessarily younger than all quiescent galaxies at the same σ. Thomas et al. (2005) show a spread in the ages of early-type galaxies at fixed σ which they can match using Monte-Carlo simulations incorporating measurements errors and an intrinsic age spread of 20–25%. Trager et al. (2000b) also show a large spread in ages at fixed σ. We have checked their reported ages as a function of [OIII] emission line strength and confirm that the galaxies in their sample with $> 2\sigma$ [OIII] emission line detections are generally younger than their quiescent galaxies at similar σ. It is possible that only a subset of LINER-like galaxies have younger ages, but these must then make up a significant fraction of the LINER-like galaxies in order to substantially lower the mean LINER-like galaxy ages to match observations.

It is also clear from Figure 12 that there cannot be a one-to-one correlation between SSP age and LINER-like emission strength because the mean Hβ age of the highest-σ LINER-like galaxies is *older* than the mean Hβ age of lower-σ quiescent galaxies; specifically, if LINER-like emission existed in all galaxies with ages below some threshold value, all LINER-like galaxies would be younger than all quiescent galaxies, regardless of σ, which is not seen. However, this trend disappears using Hδ_F, where all mean ages of LINER-like galaxies are younger than all the Hδ_F mean ages of quiescent galaxies, even though this is not true of Hβ. If, as suggested in Schiavon (2007), higher order Balmer lines are more sensitive to the presence of very young stars, this may imply that LINER-like galaxies have a larger fraction of relatively younger stars than quiescent galaxies, that is the LINER-like galaxies have had more recent star formation than their quiescent counterparts.

This does not mean that the LINER-like galaxies are post-starburst systems, galaxies which have undergone a recent epoch of powerful star formation but are no longer forming stars. Spectra of post-starburst galaxies show strong higher-order Balmer absorption lines characteristic of A stars. They are often modeled by the linear combination of an A star spectrum and a K star spectrum. The ratio of the linear coefficients of this two-component model (A/K) is used to make the post-starburst classification. Only 1.1% of the LINER-like galaxies have A/K ratios from Yan et al. (2006) consistent with identification as post-starburst galaxies ($A/K \geq 0.25$), suggesting that the LINER-like galaxy population in general is more than $\sim$ 0.5–1 Gyr beyond any major recent episode of star formation (Quintero et al. 2004). However, LINER-like galaxies might be "post post-starburst" systems seen $\gtrsim$ 1 Gyr after the post-starburst phase, possibly a continuation of the post-starburst AGN population seen in Kauffmann et al. (2003) to older ages and lower ionization AGN. It is also possible that the LINER-like galaxies are undergoing low-level star formation which is contributing to the optical emission lines.

The interpretation of the age difference between quiescent and LINER-like galaxies is not straightforward, due to the lack of consensus as to the ionization mechanism driving LINER-like emission; it is in fact likely that LINERs and LINER-like galaxies are a heterogeneous population (Filippenko 2003). Possible mechanisms for producing LINER-like emission are:

1. Photoionization by an AGN continuum (e.g., Ferland & Netzer 1983).
2. Photoionization by newly-formed O stars (e.g., Shields 1992).
3. Shock ionization (e.g., Dopita & Sutherland 1995). The shocks could be driven by starburst winds, gas accretion from a satellite galaxy or the surrounding inter-galactic medium, episodic AGN feedback, or by galaxy interactions and/or mergers.
4. Cooling flows (e.g., Heckman 1981).
5. Photoionization at early times ($\lesssim$ 500 Myr, e.g., Taniguchi, Shioya, & Murayama 2000) or at late times (1–13 Gyr, e.g., Binette et al. 1994) by post-AGB stars.

Of these possibilities, photoionization or shock ionization by young stars and photoionization by post-AGB stars are the most directly associated with the stellar population of the galaxy, and would thus give a potentially straight-forward connection between the presence of LINER-like emission and the star formation history of a galaxy. In particular, if the observed LINER-like emission in many of these galaxies is powered by young stars, it would not be at all surprising to discover that these galaxies have younger mean light-weighted ages.

However, there are several indications that this explanation is too simple. First, Yan et al. (2006) show that the LINER-like red sequence galaxies in their analysis have higher observed [OII]/Hβ ratios than either star-forming galaxies or AGN (i.e. galaxies with Seyfert-like emission line ratios), and thus LINER-like emission cannot be produced by a superposition of HII regions and AGN activity. This does not preclude the LINER-like emission being caused by star formation through a mechanism other than HII region emission, however HII regions produce strong Hβ emission and their presence would tend to weaken the [OII]/Hβ ratios of the galaxy.

There are galaxies with LINER-like emission that do show indications of containing starbursts. These are the IR-luminous galaxies described in Veilleux et al. (1995) and Sturm et al. (2006). These galaxies have mid-IR SEDs and IR fine structure emission line ratios similar to those observed in starburst galaxies (Sturm et al. 2006). In addition, they have highly reddened but intrinsically blue optical continuum colors and low Mg *b* EWs characteristic of relatively young stellar populations in dusty galaxies (Veilleux et al. 1995). We do not have mid-IR data for the SDSS galaxies to determine whether the galaxies present in our sample are indeed IR-luminous, but the optical continuum colors, internal reddening (determined by observed Hα/Hβ emission line ratios), and

Mg *b* EWs of the IR-luminous LINER-like galaxies are vastly different from those measured in the galaxy sample presented here. We therefore think it highly unlikely that these IR-luminous LINER-like galaxies contribute significantly to the LINER-like red sequence galaxies in this sample.

In the scenario where the bulk of the LINER-like emission on the red sequence is produced by post-AGB star photoionization, a correlation between LINER-like emission and stellar population age would imply that either the amount of ionizing photons produced by the old stellar population or the supply of gas (from stellar mass loss) would depend upon the age of the stars in the galaxy, which is predicted by some models (e.g., Mathews 1989).

The other possible LINER mechanisms mentioned above (photoionization by an AGN, shock ionization due to gas accretion, galaxy interactions, or merger activity, and cooling flows) are not directly related to the stellar populations of the galaxies. To explain the correlation between SSP age and emission properties with any of these mechanisms requires a connection between the stellar population age of the galaxy and some quantity external to the galaxy (accretion, interaction, cooling flows) or internal to the galaxy but separate from the stellar population (AGN activity). This would also be true of a scenario in which the post-AGB stars in the galaxy provide the ionizing photons but where the emission strength is determined by the supply of gas to be ionized, with the gas coming from an external source (rather than from stellar mass loss).

These "external" possibilities have interesting implications for galaxy evolution, in particular the possibility of ionization by low luminosity AGN. This mechanism is favored by Filippenko (2003) for centrally-concentrated LINER emission, and has a tantalizing resonance with recent work suggesting that AGN activity is involved in quenching star formation in galaxies (e.g., Kauffmann et al. 2003, Hopkins et al. 2005, Croton et al. 2006, and others). However, there is some evidence that the LINER-like emission in many if not most early-type galaxies is extended throughout the galaxy, rather than being centrally concentrated (e.g., Goudfrooij et al. 1994, Sarzi et al. 2006), suggesting that photoionization by an AGN may not be the dominant mechanism driving LINER-like emission in most early-type galaxies.

Unfortunately, it is outside the scope of this work to speculate as to which mechanism (or mechanisms) dominate the observed LINER-like emission in red sequence galaxies, making it difficult to assess the physical cause of our observed result. It would be particularly interesting to perform an analysis similar to that presented here on a sample of galaxies with spatially resolved spectra, so that true nuclear LINERs could be analyzed separately from galaxies with extended LINER-like emission.

7. CONCLUSIONS

This paper has presented an analysis of stacked spectra for a well-defined set of SDSS red sequence galaxies. Galaxies observed to harbor LINER-like emission are analyzed in parallel with quiescent galaxies, while galaxies with emission line ratios characteristic of HII regions, Seyferts, or Transition Objects have been excluded. Lick index absorption line strengths have been measured in all the stacked spectra and have been used to study the stellar population properties of red sequence galaxies as a function of galaxy velocity dispersion and emission line properties. The main results of this analysis can be summarized as follows:

1. Red sequence galaxies with LINER-like emission (roughly one-third of the total red sequence) are systematically *younger* than their quiescent counterparts at similar σ by several Gyr. Despite this age difference they appear to have metallicities and abundance patterns similar to quiescent galaxies. This result is robust to the details of the emission infill correction, the enhancement pattern of the isochrone used to construct comparison models, and the (unknown) oxygen abundance of the galaxies.

2. Many properties of red sequence galaxies' stellar populations vary with galaxy velocity dispersion, including SSP age, [Fe/H], and abundance ratios. Galaxies with higher σ are typically older and more metal-rich than lower σ galaxies, and are increasingly enhanced in Mg, C, and N. Ca appears to scale with Fe at all σ.

3. [C/Fe] and [N/Fe] vary strongly with σ; the slopes of the [C/Fe]–log σ and [N/Fe]–log σ relations are steeper than the [Mg/Fe]–log σ relation.

4. The SSP ages measured in stacked spectra from the bluer Balmer lines ($\mathrm{H}\gamma_F$ and $\mathrm{H}\delta_F$) are younger than those measured using $\mathrm{H}\beta$. This effect is not present when the S06 SSP models are used to analyze known simple stellar populations. If the interpretation presented in Schiavon (2007) is correct, the discrepant age measurements observed in this analysis indicate the presence of composite stellar populations. From the work presented here, it is not possible to tell whether the individual galaxies that go into each stacked spectrum are themselves composite stellar populations with similar star formation histories, or whether the individual galaxies are true SSPs of different ages which produce a composite population when they are combined together.

The correlation between the presence of LINER-like emission and intrinsically younger stellar populations demonstrates that there is a link between the mechanism driving the emission and the star formation history of the galaxy. If the LINER-like emission in red sequence galaxies is primarily driven by AGN activity, this may be an indication that AGN do indeed play a role in ending star formation activity. Alternatively, if the LINER-like emission in most of these galaxies is controlled entirely by the properties of the stellar population itself (e.g. gas lost from evolved stellar envelopes which is ionized by UV flux from post-AGB stars), the correlation with stellar population age may provide important constraints on models for the UV flux from low mass stars or for the rate of mass loss in a stellar population over time.

The authors wish to thank Michael R. Blanton, David W. Hogg, and collaborators for making the NYU Value-Added Galaxy Catalog publicly available. They wish to thank William G. Mathews for valuable discussion. This work was made possible by support from National Science Foundation grant AST 05-07483.

Funding for the creation and distribution of the SDSS Archive has been provided by the Alred P. Sloan Foundation, the Participating Institutions, the National Aeronautics and Space Administration, the National Science Foundation, the U.S. Department of Energy, the Japanese Monbukagakusho, and the Max Planck Society. The SDSS Web site is http://www.sdss.org/.

The SDSS is managed by the Astrophysical Research Consortium (ARC) for the Participating Institutions. The Participating Institutions are the University of Chicago, Fermilab, the Institute for Advanced Study, the Japan Participation Group, the Johns Hopkins University, the Korean Scientist Group, Los Alamos National Laboratory, the Max-Planck-Institute for Astronomy (MPIA), the Max-Planck-Institute for Astrophysics (MPA), New Mexico State University, University of Pittsburgh, University of Portsmouth, Princeton University, the United States Naval Observatory, and the University of Washington.

APPENDIX

A. CORRECTING FOR INCOMPLETENESS AT LOW σ

In §2.4, we showed that the magnitude limit of the SDSS makes the galaxy sample presented in this paper significantly incomplete in the lower σ bins, with the lowest σ bin missing as much as 51% of the galaxies it should contain. This causes the low σ bins to be increasingly biased toward the brightest galaxies in that bin.

To understand the effect of this bias on the measured line strengths, it is necessary to characterize the variation of mean absorption line strengths as a function of galaxy magnitude at fixed σ. We therefore use the total sample of 10,284 galaxies with no Hα or [O II] emission detected at the 2σ level to construct high S/N stacked spectra as a function of σ and absolute magnitude ${}^{0.1}M_r$. As in the selection of the sample of 2000 quiescent galaxies, we exclude objects with possible low-level emission and maintain a roughly symmetric distribution about EW([O II]) = 0 by requiring -3.12 Å< EW([O II]) < 3.12 Å (see §2.3). This leaves us with a sample of roughly 9400 galaxies.

These galaxies are divided into six bins in σ, as before. Each of these six bins is then divided into three bins in absolute magnitude, with equal numbers of galaxies in each magnitude bin. The median magnitudes of galaxies in the bright bins are ~ 0.5 mag brighter than those in the middle bins at the same σ, which are in turn ~ 0.5 mag brighter than those in the faint bins. Galaxies are coadded within each bin (using the process described in §2.3), and the Lick indices and D$_n$4000 are measured in each of the σ-magnitude binned spectra.

Measured line strengths are shown as a function of σ in Figure 15. In each σ range, the brightest, middle, and faintest magnitude bins are shown in red, green, and blue, respectively. As in Figure 6, error bars include statistical errors only, and the lines show a least squares fit of index strength onto σ separately for the brightest, middle, and faintest galaxies at each σ. For ease of comparison, the axis scales in each index plot are the same as in Figure 6.

From Figure 15, it is clear that the stellar populations of red sequence galaxies *do* vary with absolute magnitude at fixed σ. The iron lines (Figure 15b) in particular are considerably stronger in bright galaxies than in faint ones. However, the Balmer lines and G4300 (Figure 15a) show little variation, while other lines (Figure 15cd) show some slight variation with magnitude. This suggests that at fixed σ, brighter galaxies have higher metallicities and slightly younger ages compared to fainter galaxies.

The low σ bins of the quiescent and LINER-like galaxy sample are biased toward brighter objects and therefore, because of the variation in line strengths with magnitude, toward *stronger* absorption lines for all lines shown in Figure 15b-d. A correction for this effect is computed as follows: we assume that the characteristics of the galaxies missing from each σ bin are similar to the faint galaxies that are included in the bin, and that the mean measured properties of the bin are similar to those of the middle magnitude bin. For each measured index, the difference between the middle magnitude bin and the faint bin at fixed σ is computed by subtracting the linear fit to the middle magnitude bins (green lines in Figure 15) from the faint bins (blue lines). The line strength differential at each σ is multiplied by the corresponding incompleteness fraction (see Table 1), so that the $\sigma = 70$–120 km s^{-1} bin has the largest correction because it is most incomplete, while the $\sigma = 220$-300 bin has no correction because it is complete by assumption (see §2.4). This scaled correction is then subtracted from the measured line strengths in the quiescent, weak, and strong emission bins at each value of σ. The scaled corrections for each index are given in Table 6 for the five lowest σ bins (the highest σ bin is assumed to be complete, so no correction is applied). Implicit in this treatment is that the relative line strength differences with magnitude are the same for LINER-like galaxies as for quiescents.

The corrected line strengths are shown in Figure 6 in the right-hand column of each panel. Comparing the corrected with the uncorrected (left-hand column) values, it is clear that the corrections are small and are negligible in the Balmer lines and G4300. In the case of the metal lines (Figure 6b-d), they operate in the sense of slightly *enchancing* trends in line strength with σ. They have no effect on the relative line strengths of galaxy bins with differing emission properties because the same correction was applied to all bins at the same σ.

B. COMPARISON WITH RESULT FROM SCHIAVON 2007

Although the results presented in this work are generally consistent with the analysis of stacked SDSS spectra in Schiavon (2007), there are a number of differences worthy of deeper investigation. Schiavon (2007) finds no trend in age with galaxy luminosity when using Hβ to compute mean ages, but finds that galaxy age increases with increasing luminosity when ages are computed using Hδ_F. In contrast, we find age increasing with σ regardless of which Balmer line is used in the fitting process. In addition, Schiavon (2007) finds that [Ca/Fe] increases with galaxy luminosity, whereas we find practically no trend in [Ca/Fe] with σ. It is difficult to directly interpret these differences, as the Schiavon (2007) results are presented as a function of galaxy absolute magnitude, rather than σ.

In order to make a more direct comparison between the results of Schiavon (2007) and those presented here, we have taken the same galaxy sample used in our main analysis and divided the galaxies into bins based on absolute magnitude, rather than σ. As before, galaxies with weak and strong LINER-like emission are stacked separately from those with no detectable emission lines. For this process, we have used the galaxy absolute r-band magnitude, K-corrected to z=0.0 in order to match the Schiavon (2007) data which made use of stacked spectra from Eisenstein et al. (2003). We then measure Lick indices and fit for stellar population mean ages, abundances, and abundance ratios as described in §3 and §4 above.

Figure 16 shows the results of the stellar population modeling for our luminosity-binned sample (black stars), as compared to the results from Schiavon (2007) (grey triangles). Values of [Fe/H] appear slightly higher in the Schiavon (2007) results than in our luminosity-binned sample, by a few hundredths of a dex. The typical values for the abundance ratios are comparable between the two data sets, but the Schiavon (2007) values show consistently stronger trends with magnitude than do our data. Again, the discrepancies are all within a few hundredths of a dex. The largest discrepancies between the data sets are in the age measurements. Here our data show slightly older ages for more luminous galaxies, while the Schiavon (2007) results show slightly *younger* ages for more luminous galaxies.

Because both the Eisenstein et al. (2003) stacked spectra and the stacked spectra in our sample were acquired as part of the same survey and have been analyzed using the same method, any differences in the results should be due to differences in the sample selection process. The sample selection criteria are in fact quite different between the two samples. Both samples are taken from the SDSS MAIN galaxy sample. The Eisenstein et al. (2003) spectra used in Schiavon (2007) are chosen using two morphological criteria: that the galaxies have concentrated light profiles (determined from the SDSS concentration parameter c, see Eisenstein et al. 2003 for details) and by requiring that a de Vaucouleurs fit to the light profile be 20 times more likely than an exponential fit. Most of these galaxies lie on the red sequence; an additional color criterion is applied to exclude color outliers, removing about 5% of the morphologically selected galaxies from the sample.

It is important to highlight here that no spectral criteria are applied. Many of the galaxies in the Eisenstein et al. (2003) stacked spectra may therefore include emission lines from ionized gas. In fact, the principle component analysis in Eisenstein et al. (2003) shows that there is a significant component of emission in the galaxies in their sample. Yan et al. (2006) have shown that red sequence galaixes (chosen by a color criterion only, without any morphological selection) consist of about 48% quiescent galaxies without emission lines, 29% galaxies with LINER-like emission, and 23% galaxies with emission characteristic of Seyferts or HII regions. The morphological selection applied by Eisenstein et al. (2003) may remove some fraction of the Seyferts and star-forming galaxies from the red sequence, but a contaminating population of galaxies with emission due to low-level star formation or Seyfert activity likely exists at the roughly 10% level.

Before measured Lick indices and analyzing the stellar populations of the stacked Eisenstein et al. (2003) spectra, Schiavon (2007) corrects for emission infill in the stacked spectra by measuring the strength of the [OII]λ3727 line and applying the conversion from [OII] EW to Hα EW determined in Yan et al. (2006). A standard Balmer decrement is then used to correct Hβ, Hγ_F, and Hδ_F. However, this conversion is appropriate only for galaxies with LINER-like emission line ratios. The Eisenstein et al. (2003) spectra may contain some fraction of Seyferts and low-level star formation. For these galaxies, the strength of Hα emission is much higher for a given [OII] EW, thus the emission infill correction performed by Schiavon (2007) may *undercorrect* for infill in the Balmer lines, to the extent that galaxies in the sample have non-LINER-like emission line ratios. As discussed in §3.3, Hβ will be much more sensitive to the effects of infill than will the bluer Balmer lines.

Figure 17 shows Lick index measurements as a function of galaxy absolute magnitude for our sample (black stars) and for the Eisenstein et al. (2003) stacked spectra (grey triangles). Only Lick indices that are used in the abundance fitting process are shown. The Balmer lines (left panel) differ significantly between the two data sets, while the metal lines Fe5270, Fe5335, Mg b, $C_2$4668, CN_2, and Ca4227 are relatively consistent. In our luminosity-binned data, all three Balmer line strengths decrease as galaxy luminosity increases. The same trend is seen in Hδ_F and Hγ_F for the Eisenstein et al. (2003) data, although the line strengths are offset toward stronger absorption compared to our data. This suggests that the Eisenstein et al. (2003) sample of galaxies includes a larger fraction of intermediate-age galaxies than does our own.

This offset in mean stellar population age between the samples is not unexpected. The galaxies included in our luminosity-binned sample, as in the σ-binned sample used in the main analysis presented above, have been selected with a fairly stringent color cut, which excludes the blue side of the red sequence (see Figure 1). No such stringent cut has been applied to the Eisenstein et al. (2003) galaxies. That sample therefore contains a sizable fractin of galaxies which are as much as 0.1 mag bluer in $g - r$ than our galaxy sample and therefore may include a significant sub-population of intermediate-age galaxies which are excluded from our sample.

Also, as discussed earlier, the Eisenstein et al. (2003) data likely include a modest fraction of galaxies with low-level star formation because galaxies have not been excluded on the basis of emission lines. Including these galaxies would bias the sample toward younger mean ages. It is true that the star-forming galaxies also have stronger Balmer emission infill, which we have argued is likely to be under-corrected. However, the effect on the blue Balmer lines is small both in terms of the total amount of infill and the amount of correction applied, thus the inaccuracies in accounting for the infill in Hδ_F and Hγ_F should not be large.

This is not true for Hβ, where the emission infill is substantial and therefore the effect of the under-correction could be significant. Indeed, Hβ behaves differently in the Eisenstein et al. (2003) stacked spectra than in our luminosity-binned spectra; Hβ remains roughly constant over a range of galaxy absolute magnitude in the Eisenstein et al. (2003) data whereas Hβ strengths decline for brighter galaxies in our sample. The contant values of Hβ are also qualitatively different from the Hδ_F and Hγ_F indices in both the Eisenstein et al. (2003) data and in our data, where Balmer absorption declines with increasing galaxy luminosity everywhere. It seems likely that the Hβ values measured in the Eisenstein et al. (2003) data suffer from an improper infill correction which has dramatic effects on Hβ but less so on Hδ_F and Hγ_F, and none at all on the metal lines.

The metal lines in fact appear very similar between the two different data sets. There is some indication that metal absorption strengths are slightly lower in the Eisenstein et al. (2003) data, which would be consistent with the supposition that those data include a larger fraction of intermediate-age galaxies than do our data. The slopes of the relations between line strengths and galaxy magnitude are in good agreement between the two samples.

We therefore conclude that the slight differences in the ages and abundance patterns reported by Schiavon (2007) as compared to the results presented in this paper are due to differing trends in the Hβ line strengths that are used to compute the fiducial galaxy ages (see §4), rather than genuine differences in abundance patterns. These differing trends in measured Hβ line strengths are due to differences in sample selection coupled with less accurate emission infill corrections applied to the Eisenstein et al. (2003) data in Schiavon (2007). In order for this to explain the observed flat relationship between Hβ absorption strength and galaxy luminosity, the fainter galaxies would have to be more affected by under-corrected emission infill (in other words, the fainter galaxies would have to have a larger fraction of galaxies with emission having non-LINER-like line ratios). It seems reasonable that the fainter Eisenstein et al. (2003) galaxies, which are observed to have much stronger Hδ_F absorption than the brighter galaxies, are more likely to contain residual star formation and weak HII region emission than the brighter galaxies.

It should be noted that the differences in abundances shown in Figure 16 between the two data sets are never more than 0.05 dex. Although different sample selection and inaccurate emission infill corrections pose problems for precision stellar population determinations, there does not seem to be a catastrophic discrepancy created by moderate differences in the input data.

REFERENCES

Adelman-McCarthy, J. K. et al. 2006, ApJS, 162, 38
Baldwin, J. A., Phillips, M. M., & Terlevich, R. 1981, PASP, 93, 5
Balogh, M. L., Morris, S. L., Yee, H. K. C., Carlberg, R. G., & Ellingson, E. 1999, ApJ, 527, 54
Barbuy, B., Meléndez, J., Ortolani, S., Zoccali, M., Bica, E., Renzini, A., Hill, V., Momany, Y., Minniti, D., & Rich, M. 2004, Memorie della Societa Astronomica Italiana, 75, 398
Bell, E. F., Wolf, C., Meisenheimer, K., Rix, H.-W., Borch, A., Dye, S., Kleinheinrich, M., Wisotzki, L., & McIntosh, D. H. 2004, ApJ, 608, 752
Bender, R., Burstein, D., & Faber, S. M. 1992, ApJ, 399, 462
Bernardi, M., Sheth, R. K., Nichol, R. C., Schneider, D. P., & Brinkmann, J. 2005, AJ, 129, 61
Bernardi, M., et al. 2003a, AJ, 125, 1817
Bernardi, M., et al. 2003b, AJ, 125, 1882
Binette, L., Magris, C. G., Stasinska, G., & Bruzual, A. G. 1994, A&A, 292, 13
Blanton, M. R., et al. 2003a, AJ, 125, 2348
Blanton, M. R., et al. 2003b, ApJ, 594, 186
Blanton, M. R., et al. 2005, AJ, 129, 2562
Bruzual, G. & Charlot, S. 2003, MNRAS, 344, 1000
Caon, N., Macchetto, D., & Pastoriza, M. 2000, ApJS, 127, 39
Cardiel, N., Gorgas, J., Cenarro, J., & González, J. J. 1998, A&AS, 127, 597
Carollo, C. M., Danziger, I. J., & Buson, L. 1993, MNRAS, 265, 553
Carretta, E., Cohen, J. G., Gratton, R. G., & Behr, B. B. 2001, AJ, 122, 1469
Cenarro, A. J., Gorgas, J., Vazdekis, A., Cardiel, N., & Peletier, R. F. 2003, MNRAS, 339, L12
Clemens, M. S., Bressan, A., Nikolic, B., Alexander, P., Annibali, F., & Rampazzo, R. 2006, MNRAS, 370, 702
Cowie, L. L., Songaila, A., Hu, E. M., & Cohen, J. G. 1996, AJ, 112, 839
Croton, D. J., et al. 2006, MNRAS, 365, 11
Denicoló, G., Terlevich, R., Terlevich, E., Forbes, D., Terlevich, A., & Carrasco, L. 2005, MNRAS, 356, 1440
Denicoló, G., Terlevich, R., Terlevich, E., Forbes, D., & Terlevich, A. 2005, MNRAS, 358, 813
Dopita, M. A., & Sutherland, R. S. 1995, ApJ, 455, 468
Dopita, M. A., & Sutherland, R. S. 1996, ApJS, 102, 161
Eisenstein, D. J. et al. 2003, ApJ, 585, 694
Faber, S. M., & Jackson, R. E. 1976, ApJ, 204, 668
Faber, S. M., et al. 2006, astro-ph/0506044
Ferland, G. J., & Netzer, H. 1983, ApJ, 264, 105
Filippenko, A. V. 2003, ASPC, 290, 369 (astro-ph/0307137)
Fukugita, M., Ichikawa, T., Gunn, J. E., Doi, M., Shimasaku, K., & Schneider, D. P. 1996, AJ, 111, 1748
Fulbright, J. P., McWilliam, A., & Rich, R. M. 2006, astro-ph/0609087
Girardi, L., Bressan, A., Bertelli, G., & Chiosi, C. 2000, A&AS, 141, 371
González, J. J. 1993, PhD Thesis, University of California at Santa Cruz
Gorgas, J., Faber, S. M., Burstein, D., González, J. J., Courteau, S., & Prosser, C. 1993, ApJS, 86, 153
Goudfrooij, P. 1999, in ASP Conf. Ser. 163: "Star Formation in Early-Type Galaxies", Eds. J. Cepa & P. Carral, 163, 55 (astro-ph/9809057)
Goudfrooij, P., Hansen, L., Jørgensen, H. E., & Nørgaard-Nielsen, H. U. 1994, A&AS, 105, 341
Graves, G. J., & Schiavon, R. P. 2007, in preparation
Grevesse, N., Noels, A., & Sauval, A. J. 1996, in ASP Conf. Ser. 99: "Cosmic Abundances", ed. S. S. Holt & G. Sonneborn (San Francisco: ASP), 117
Halpern, J. P., & Steiner, J. E. 1983, ApJ, 269, 37
Harker, J. J., Schiavon, R. P., Weiner, B. J., & Faber, S. M. 2006, ApJ, 647, L103
Heckman, T. M. 1980, A&A, 87, 152
Heckman, T. M. 1981, ApJ, 250, 59
Ho, L. C., Filippenko, A. V., & Sargent, W. L. 1995, ApJS, 98, 477
Ho, L. C., Filippenko, A. V., & Sargent, W. L. 1997, ApJ, 487, 568
Hopkins, P. F., Hernquist, L., Cox, T. J., Di Matteo, T., Martini, P., Robertson, B., & Springel, V. 2005, ApJ, 630, 705
Humphrey, P. J., & Buote, D. A. 2006, ApJ, 639, 136
Humphrey, P. J., Buote, D. A., & Canizares, C. R. 2004, ApJ, 617, 1047
Jørgensen, I., Franx, M., & Kjærgaard, P. 1995, MNRAS, 276, 1341
Jordi, K., Grebel, E. K., & Ammon, K. 2006, A&A, 460, 339
Kauffmann, G. et al. 2003, MNRAS, 346, 1055
Kaviraj, S. et al. 2006, astro-ph/0601029
Kewley, L., Dopita, M., Sutherland, R., Heisler, C., & Trevena, J. 2001, ApJ, 556, 121
Kim, D.-C., Sanders, D. B., Veilleux, S., Mazzarella, J. M., & Soifer, B. T. 1995, ApJS, 98, 129
Korn, A. J., Maraston, C., & Thomas, D. 2005, A&A, 438, 685
Kuntschner, H., et al. 2006, MNRAS, 369, 497
Macchetto, F., Pastoriza, M., Caon, N., Sparks, W. B., Giavalisco, M., Bender, R., & Capaccioli, M. 1996, A&A, 120, 463
Mathews, W. G. 1989, AJ, 97, 42
Nelan, J. E., Smith, R. J., Hudson, M. J., Wegner, G. A., Lucey, J. R., Moore, S. A. W., Quinney, S. J., & Suntzeff, N. B. 2005, ApJ, 623, 137
Noeske, K. G., Faber, S. M., Weiner, B. J., Koo, D. C., Primack, J. R., Dekel, A., Papovich, C., Conselice, C. J., Le Floc'h, E., Rieke, G. H., Coil, A. L., Lotz, J. M., Somerville, R. S., & Bundy, K. 2007, astro-ph/0703056
O'Connell, R. W. 1976, ApJ, 206, 370
Ogando, R. L. C., Maia, M. A. G., Chiappini, C., Pellegrini, P. S. S., Schiavon, R. P., & da Costa, L. N. 2006, RevMexAA, 26, 119

Osterbrock, D. E., & Ferland, G. J. 2005, Astrophysics of Gaseous Nebulae and Active Galactic Nuclei, Second Edition (Sausalito: University Science Books)

Prochaska, L. C., Rose, J. A., & Schiavon, R. S. 2005, AJ, 130, 2666

Quintero, A. D., et al. 2004, ApJ, 602, 190

Rampazzo, R., Annibali, F., Bressan, A., Longhetti, M., Padoan, R., & Zeilinger, W. W. 2005, A&A, 433, 497

Saglia, R. P., Maraston, C., Thomas, D., Bender, R., & Colless, M. 2002, ApJ, 579, L13

Salasnich, B., Girardi, L., Weiss, A., & Chiosi, C. 2000, A&A, 361, 1023

Sánchez-Blázquez, P., Gorgas, J., Cardiel, N., & González, J. J. 2006, A&A, 457, 809

Sarzi, M. et al. 2006, MNRAS, 366, 1151

Schawinski, K. et al. 2006, astro-ph/0601036

Schiavon, R. P. 2007, ApJS, 171, 146

Schiavon, R. P., et al. 2006, ApJ, 651, L93

Serven, J., Worthey, G., & Briley, M. M. 2005, ApJ, 627, 754

Shields, J. C. 1992, ApJ, 399, 27

Smith, R. J., Lucey, J. R., & Hudson, M. J., submitted to MNRAS

Stoughton, C., et al. 2002, AJ, 123, 485

Sturm, E., et al. 2006, ApJ, 653, L13

Taniguchi, Y., Shioya, Y., & Murayama, T. 2000, AJ, 120, 1265

Thomas, D., Maraston, C., Bender, R., Mendes de Oliveira, C. 2005, ApJ, 621, 673

Thomas, D., Maraston, C., & Bender, R. 2003, MNRAS, 339, 897

Thomas, D., Maraston, C., & Korn, A. 2004, MNRAS, 351, L19

Trager, S. C., Faber, S. M., Worthey, G. & González, J. J. 2000, AJ, 119, 1645

Trager, S. C., Faber, S. M., Worthey, G., & González, J. J. 2000, AJ, 120, 165

Treu, T., Ellis, R. S., Liao, T. X., & van Dokkum, P. G. 2005, ApJ, 622, L5

Veilleux, S., Kim, D.-C., Sanders, D. B., Mazzarella, J. M., & Soifer, B. T. 1995, ApJS, 98, 171

Vandenberg, D. A. & Bell, R. A. 2001, New A Rev, 45, 577

Vazdekis, A., Peletier, R. F., Beckman, J. E., & Casuso, E. 1997, ApJS, 111, 203

Wheeler, J. C., Sneden, C., & Truran, J. W. 1989, ARA&A, 27, 279

Woosley, S. E., & Weaver, T. A. 1995, ApJS, 101, 181

Worthey, G. 1998, PASP, 110, 888

Worthey, G., Faber, S. M., González, J. J., & Burstein, D. 1994, ApJS, 94, 687

Worthey, G., & Ottaviani, D. L. 1997, ApJS, 111, 377

Yan, R., Newman, J. A., Faber, S. M., Konidaris, N., Koo, D., & Davis, M. 2006, ApJ, 648, 281

Yi, S. K., et al. 2005, ApJ, 619, L111

Zoccali, M., Barbuy, B., Hill, V., Ortolani, S., Renzini, A., Bica, E., Momany, Y., Pasquini, L., Minniti, D., & Rich, M. 2004, A&A, 423, 507

TABLE 1
Stacked Spectra: Parameters

σ (km s^{-1})	Fractional Incompleteness	LINER emission	#	$S/N_{\rm med}$ (Å^{-1})	$\langle\sigma\rangle$ (km s^{-1})	$\langle$EW[OII]$\rangle$ (Å)
70–120	51%	quiescent	339	298.0	103.2	-0.02
		weak	137	229.1	105.9	3.75
		strong	317	280.2	101.7	9.10
120–145	28%	quiescent	374	366.9	133.4	0.12
		weak	248	344.7	133.8	3.63
		strong	388	379.5	133.5	8.40
145–165	19%	quiescent	327	389.5	155.2	-0.03
		weak	286	408.8	155.8	3.44
		strong	369	420.3	155.2	8.90
165–190	11%	quiescent	307	405.7	176.5	-0.23
		weak	380	521.5	177.4	3.38
		strong	394	485.1	176.7	8.64
190–220	4%	quiescent	317	469.7	204.1	-0.11
		weak	374	561.9	203.9	3.25
		strong	347	506.7	203.2	9.06
220–300	...	quiescent	284	526.4	245.8	-0.27
		weak	289	570.9	247.1	3.14
		strong	326	550.6	243.6	9.67

TABLE 2
Indices in Stacked Spectra: Balmer Indices*

Name	Hβ (Å)			Hγ_F (Å)			Hδ_F (Å)		
Infill Correction:**	Ho97	Yan06	none	Ho97	Yan06	none	Ho97	Yan06	none
70–120 / quiescent	1.88	1.88	1.88	-0.90	-0.90	-0.90	0.58	0.58	0.58
70–120 / weak	1.95	1.90	1.69	-0.45	-0.48	-0.61	1.04	1.02	0.95
70–120 / strong	2.15	2.03	1.47	-0.03	-0.12	-0.45	1.39	1.33	1.14
120–145 / quiescent	1.79	1.79	1.79	-1.06	-1.06	-1.06	0.53	0.53	0.53
120–145 / weak	1.93	1.89	1.67	-0.68	-0.72	-0.85	0.93	0.91	0.83
120–145 / strong	2.04	1.93	1.43	-0.47	-0.55	-0.85	1.03	0.98	0.80
145–165 / quiescent	1.78	1.78	1.78	-1.24	-1.24	-1.24	0.49	0.49	0.49
145–165 / weak	1.87	1.82	1.62	-0.89	-0.92	-1.04	0.79	0.77	0.69
145–165 / strong	1.98	1.85	1.32	-0.73	-0.82	-1.15	0.85	0.80	0.61
165–190 / quiescent	1.73	1.73	1.73	-1.33	-1.33	-1.33	0.47	0.47	0.47
165–190 / weak	1.83	1.78	1.58	-1.07	-1.11	-1.23	0.70	0.68	0.60
165–190 / strong	1.93	1.81	1.29	-0.98	-1.07	-1.39	0.73	0.68	0.49
190–220 / quiescent	1.70	1.70	1.70	-1.45	-1.45	-1.45	0.32	0.32	0.32
190–220 / weak	1.73	1.68	1.49	-1.29	-1.32	-1.44	0.51	0.49	0.42
190–220 / strong	1.83	1.70	1.16	-1.19	-1.28	-1.63	0.63	0.57	0.37
220–300 / quiescent	1.63	1.63	1.63	-1.61	-1.61	-1.61	0.22	0.22	0.22
220–300 / weak	1.63	1.59	1.40	-1.51	-1.54	-1.66	0.35	0.33	0.26
220–300 / strong	1.72	1.58	1.01	-1.41	-1.51	-1.88	0.47	0.40	0.18

---

* Index values are as measured in the stacked spectra. They do *not* include the corrections for incompleteness described in Appendix A** Balmer index measurements are shown for three different choices of emission infill correction: (1) assuming Hα/Hβ = 3.27 as in Ho, Filippenko, & Sargent (1997), (2) assuming Hα/Hβ = 4.1 as in Yan et al. (2006), and (3) with no infill correction. See §2.2 for details.

TABLE 3
Indices in Stacked Spectra: D$_n$4000, Fe, and Mg Indices[*]

Name	D$_n$4000	Fe4383 (Å)	Fe4531 (Å)	Fe5270 (Å)	Fe5335 (Å)	Fe5406 (Å)	Mg$_1$ (mag)	Mg$_2$ (mag)	Mg *b* (Å)
70–120 / quiescent	1.87	3.92	2.89	2.64	2.32	1.56	0.080	0.205	3.43
70–120 / weak	1.81	3.83	2.87	2.50	2.25	1.52	0.075	0.195	3.38
70–120 / strong	1.76	3.52	2.83	2.49	2.18	1.46	0.069	0.182	3.13
120–145 / quiescent	1.91	4.19	3.06	2.70	2.39	1.62	0.091	0.223	3.76
120–145 / weak	1.85	3.99	2.99	2.70	2.40	1.64	0.085	0.213	3.62
120–145 / strong	1.82	3.92	2.99	2.65	2.29	1.50	0.083	0.206	3.58
145–165 / quiescent	1.94	4.28	3.03	2.71	2.46	1.64	0.100	0.237	3.91
145–165 / weak	1.89	4.16	3.04	2.70	2.45	1.63	0.094	0.225	3.76
145–165 / strong	1.87	4.13	3.03	2.69	2.42	1.60	0.093	0.222	3.82
165–190 / quiescent	1.96	4.25	3.13	2.74	2.53	1.67	0.105	0.244	4.10
165–190 / weak	1.90	4.25	3.10	2.75	2.47	1.65	0.100	0.237	4.02
165–190 / strong	1.92	4.31	3.07	2.76	2.46	1.66	0.103	0.239	4.05
190–220 / quiescent	1.99	4.35	3.16	2.81	2.52	1.73	0.114	0.254	4.16
190–220 / weak	1.99	4.42	3.19	2.79	2.57	1.70	0.112	0.256	4.27
190–220 / strong	1.98	4.40	3.15	2.70	2.50	1.67	0.112	0.252	4.27
220–300 / quiescent	2.06	4.48	3.28	2.81	2.65	1.70	0.126	0.276	4.55
220–300 / weak	2.01	4.54	3.23	2.85	2.64	1.77	0.125	0.270	4.45
220–300 / strong	1.99	4.45	3.23	2.84	2.58	1.75	0.126	0.271	4.56

[*] Index values are as measured in the stacked spectra. They do *not* include the corrections for incompleteness described in Appendix A

TABLE 4
Indices in Stacked Spectra: CN, CH, C$_2$, Ca, Na, and TiO Indices[*]

Name	CN$_1$ (mag)	CN$_2$ (mag)	G4300 (Å)	C$_2$4668 (Å)	Ca4227 (Å)	Ca4455 (Å)	NaD (Å)	TiO$_1$ (mag)	TiO$_2$ (mag)
70–120 / quiescent	0.0263	0.0507	4.83	5.40	0.95	1.12	2.61	0.0248	0.0612
70–120 / weak	0.0139	0.0398	4.56	5.06	0.83	1.02	2.64	0.0246	0.0604
70–120 / strong	-0.0051	0.0207	4.19	4.63	0.86	0.97	2.77	0.0246	0.0573
120–145 / quiescent	0.0386	0.0659	4.99	5.70	0.99	1.16	3.08	0.0271	0.0643
120–145 / weak	0.0261	0.0528	4.74	5.62	0.93	1.07	2.98	0.0234	0.0627
120–145 / strong	0.0184	0.0451	4.59	5.26	0.91	1.07	3.24	0.0238	0.0614
145–165 / quiescent	0.0468	0.0742	5.05	6.02	1.00	1.21	3.18	0.0280	0.0677
145–165 / weak	0.0377	0.0639	4.82	5.91	0.94	1.16	3.41	0.0241	0.0655
145–165 / strong	0.0357	0.0626	4.85	5.68	0.93	1.10	3.40	0.0249	0.0650
165–190 / quiescent	0.0559	0.0859	5.17	6.13	0.97	1.21	3.18	0.0254	0.0689
165–190 / weak	0.0487	0.0769	4.96	6.22	0.96	1.18	3.48	0.0256	0.0675
165–190 / strong	0.0478	0.0763	4.97	6.06	0.95	1.14	3.50	0.0265	0.0689
190–220 / quiescent	0.0694	0.1025	5.22	6.55	1.02	1.23	3.62	0.0286	0.0713
190–220 / weak	0.0640	0.0938	5.11	6.63	1.02	1.21	3.83	0.0280	0.0711
190–220 / strong	0.0629	0.0929	5.14	6.43	1.01	1.21	3.96	0.0272	0.0712
220–300 / quiescent	0.0896	0.1233	5.32	6.91	1.08	1.32	4.16	0.0321	0.0762
220–300 / weak	0.0842	0.1168	5.20	6.99	1.03	1.28	4.47	0.0305	0.0754
220–300 / strong	0.0823	0.1134	5.20	6.87	1.03	1.26	4.41	0.0290	0.0744

[*] Index values are as measured in the stacked spectra. They do *not* include the corrections for incompleteness described in Appendix A

TABLE 5
Direction of Line Strength Change in SSP Models

	Balmer lines	D$_n$4000, G4300	Metal lines
Age ⇑	⇓	⇑	⇑
[Fe/H] ⇑	⇓	⇑	⇑

TABLE 6
Incompleteness Corrections

Index	σ bin 70–120 km s^{-1}	σ bin 120–145 km s^{-1}	σ bin 145–165 km s^{-1}	σ bin 165–190 km s^{-1}	σ bin 190–220 km s^{-1}
D$_n$4000	0.0255	0.0089	0.0041	0.0013	0.0001
Hδ_F	0.0240	0.0030	-0.0020	-0.0032	-0.0020
CN$_1$	0.0032	0.0014	0.0009	0.0004	0.0001
CN$_2$	0.0038	0.0016	0.0009	0.0004	0.0001
Ca4227	0.0058	0.0059	0.0050	0.0035	0.0015
G4300	0.0292	0.0112	0.0057	0.0023	0.0005
Hγ_F	-0.0698	-0.0255	-0.0123	-0.0045	-0.0006
Fe4383	0.0765	0.0456	0.0324	0.0195	0.0074
Ca4455	0.0069	0.0071	0.0061	0.0042	0.0018
Fe4531	0.0298	0.0153	0.0100	0.0055	0.0019
C$_2$4668	0.2019	0.1160	0.0807	0.0478	0.0178
Hβ	0.0104	0.0103	0.0088	0.0060	0.0025
Mg$_1$	0.0019	0.0008	0.0004	0.0002	0.0001
Mg$_2$	0.0054	0.0023	0.0013	0.0006	0.0002
Mg b	0.0873	0.0328	0.0164	0.0064	0.0011
Fe5270	0.0474	0.0303	0.0222	0.0137	0.0053
Fe5335	0.0476	0.0286	0.0203	0.0123	0.0047
Fe5406	0.0382	0.0187	0.0118	0.0064	0.0021
NaD	0.1200	0.0563	0.0345	0.0180	0.0058
TiO$_1$	-0.0017	-0.0006	-0.0002	-0.0001	0.0000
TiO$_2$	0.0006	0.0004	0.0003	0.0002	0.0001

Note. — Values given are the scaled corrections for incompleteness, as described in §A. These are *subtracted* from the measured index strengths given in Table 2. The same correction is applied to quiescent, weak, and strong LINER-like emission composite spectra. All incompleteness corrections are given in the units of the corresponding index (CN$_1$, CN$_2$, Mg$_1$, Mg$_2$, TiO$_1$, and TiO$_2$ are in magnitudes, D$_n$4000 is dimensionless, and all others are in Å).

TABLE 7
Abundance Trends with σ

Abundance $= a + b \log \sigma$

Abundance	b	a
[Fe/H]	0.451 ± 0.034	-1.14 ± 0.08
[Mg/Fe]	0.362 ± 0.043	-0.61 ± 0.10
[C/Fe]	0.555 ± 0.027	-1.06 ± 0.06
[N/Fe]	0.640 ± 0.035	-1.34 ± 0.08
[Ca/Fe]	0.130 ± 0.039	-0.29 ± 0.09
[Z/H] ([O/Fe] = 0.0)	0.786 ± 0.050	-1.80 ± 0.11
[Z/H] ([O/Fe] = 0.3)	0.705 ± 0.051	-1.47 ± 0.11
[Z/H] ([O/Fe] = 0.5)	0.656 ± 0.052	-1.23 ± 0.12
[Z/H] ([O/Fe] = [Mg/Fe])	0.916 ± 0.054	-2.00 ± 0.12
[Z/H] ([O/Fe] = [Mg/Fe] + 0.3)	0.895 ± 0.055	-1.77 ± 0.12

TABLE 8

TRENDS WITH σ: COMPARISON WITH OTHER WORK

$\log Age = a + b \log \sigma$ $Abundance = a + b \log \sigma$		This Work	Trager et al. (2000b)	Thomas et al. (2005)	Nelan et al. (2005)	Smith et al. (2007)	Bernardi et al. (2003b)
Age	b	0.35 ± 0.03[b]	0.6 ± 0.2[c]	0.24 (0.32)[d]	0.59 ± 0.13	0.52 ± 0.06	1.15
[Fe/H]	b	0.45 ± 0.03	0.48 ± 0.12[c]	...	...	...	...
[Z/H]	b	0.79 ± 0.05[e]	0.76 ± 0.13[c]	0.55 (0.57)[d]	0.53 ± 0.08	0.34 ± 0.04	0.38
[α/Fe][a]	b	0.36 ± 0.04	0.33 ± 0.01	0.28 (0.28)[d]	0.31 ± 0.06	0.23 ± 0.04	0.32
SSP Models[f]		S06	W94	TMB03	TMB03	TMB03	TMB03

[a] Measured using Mg b in all works except Nelan et al.(2005) which uses Mg b and CN_1 as α sensitive indices. Corresponds to [Mg/Fe] in this work.[b] From fit to Hβ age, quiescent galaxies only.[c] Trager et al.(2000b) posit the existence of an "age-metallicity hyperplane" such that galaxies display a range of ages and [Z/H] (or [Fe/H]) at fixed σ, with an *anticorrelation* between age and [Z/H]; they therefore give [Z/H] as a function of σ and age. The age relation given here is from the Nelan et al.(2005) fit to the Trager et al. data, while the [Z/H] and [Fe/H] values include only the σ portion of the effect on [Z/H] and [Fe/H] reported in Trager et al.(2005b), ignoring the effect of age.[d] Thomas et al.(2005) report two sets of relations for galaxies in low and high density environments. Values for both environments are show as: high density (low density).[e] Calculated with [O/Fe] = 0.0, as described in §5.3. For other choices of [O/Fe], see Table 5.[f] S06: Schiavon (2007), W94: Worthey et al. (1994), TMB03: Thomas, Maraston, & Bender (2003)

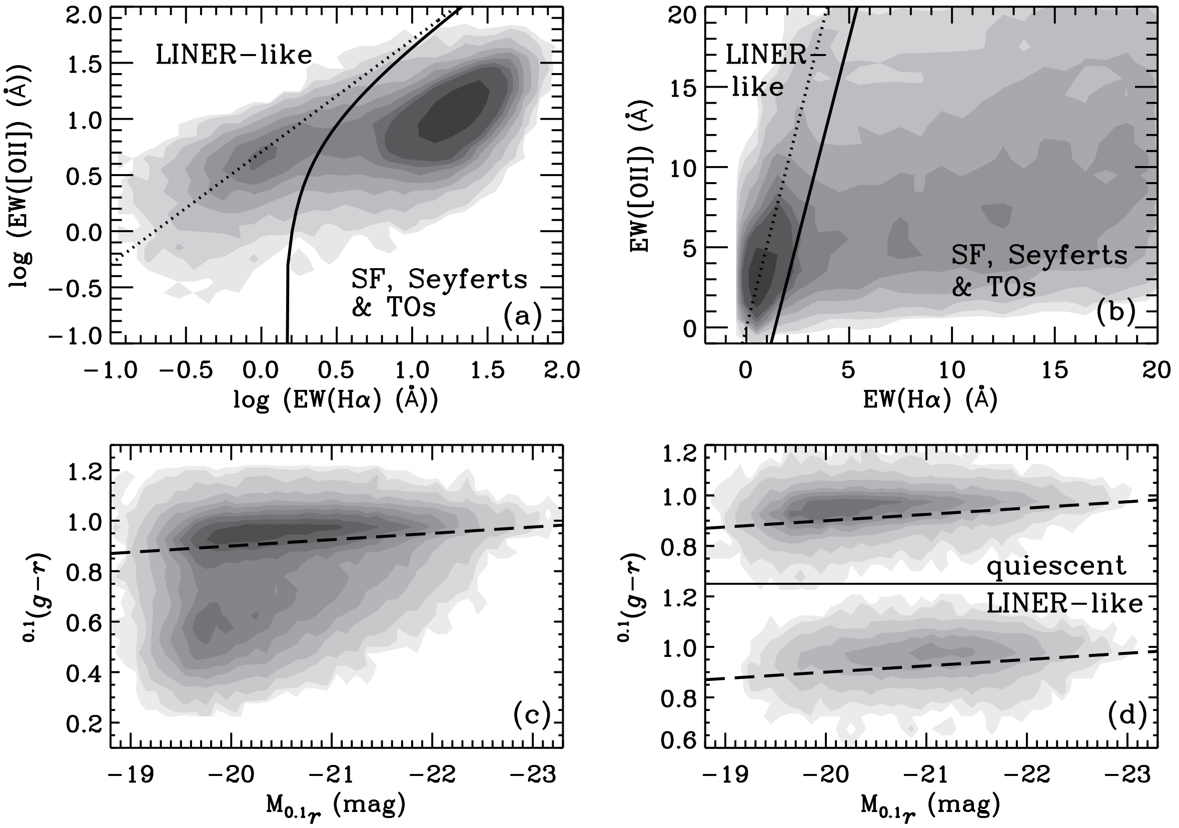

FIG. 1.— (a) Hα and [OII] EWs for all galaxies in the redshift range $0.06 < z < 0.08$ and with both lines detected at $> 2\sigma$. The distribution is bimodal (see Yan et al. 2006 for details). The EW(Hα)/EW([OII]) criterion of equation 2 is used to define the LINER-like sample is shown as the solid line. Galaxies to the right of the solid line were discarded as "Low-[OII]/Hα"contaminants with dusty star formation, Seyfert emission, or a mixture of Seyfert and star forming emission (Transition Objects). The dashed line shows the linear least squares fit of EW(Hα) as a function of EW([OII]) which was used to convert a measured [OII] EW into an Hα EW as part of the infill-correction process (see §2.2). (b) The same as (a) but with linear-scaled axes. (c) Color-magnitude diagram of all SDSS galaxies in the redshift range $0.06 < z < 0.08$. The dashed line shows eq. 1 used to define the red sequence galaxies included in the sample. (d) Color-magnitude diagram of LINER-like and quiescent galaxies selected for the sample presented here. The dashed line shows the cut used to define the red sequence. The LINER-like and quiescent samples have similar color distributions (mostly red sequence galaxies) but different magnitude distributions. See text for details. In all panels, contour levels in all panels indicate the density of objects in the plot corresponding to, from light to dark, 3, 10, 30, 60, 100, 150, 200, 300, 400 galaxies per bin, where bin boundaries correspond to the tickmarks shown on the x and y axes.

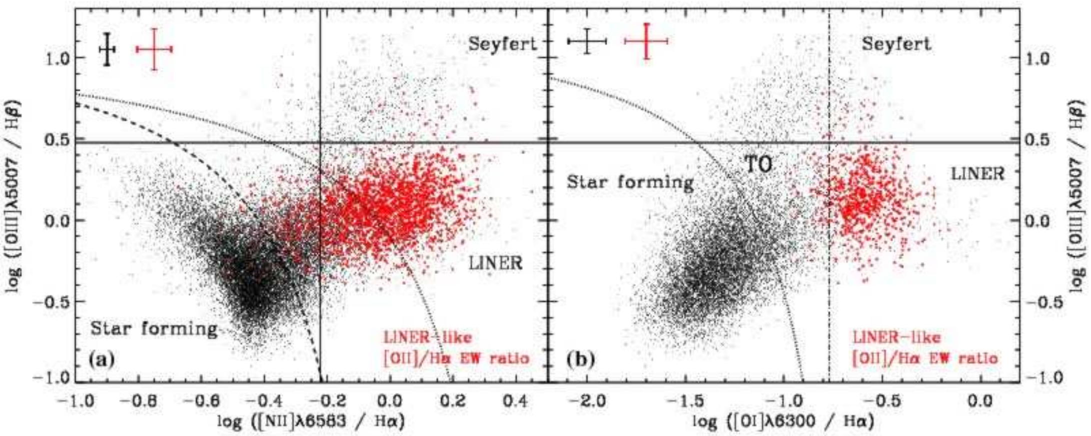

Fig. 2.— BPT diagrams (Baldwin, Phillips, & Terlevich 1981) for galaxies with $0.06 < z < 0.08$. Red points show those galaxies classified as "LINER-like" in our sample based on their EW([OII])/EW(Hα) ratios; black points show all other galaxies. Only galaxies with all four emission lines detected at the 3σ level are plotted in each panel. The weak [OI] emission line is undetected in many galaxies, thus (b) contains fewer galaxies than (a). Error bars in the upper left show the median error in line ratios separately for the LINER-like and other galaxies. The solid lines show the standard classification scheme: Seyferts have [OIII]/H$\beta > 3$ and [NII]/H$\alpha > 0.6$, LINERs have [OIII]/H$\beta < 3$ and [NII]/H$\alpha > 0.6$, and star forming galaxies have [NII]/H$\alpha < 0.6$. Dotted lines show the separation of Kewley et al. (2001) between star forming galaxies and active nuclei; the dashed line in (a) shows the Kauffmann et al. (2003) separation. The dash-dot line in (b) shows the Ho, Filippenko, & Sargent (1997) separation between LINERs and transition objects (TOs). Using the Kauffmann et al. (2003) separation between star forming galaxies and active nuclei, the standard separation between Seyferts and LINERs, and the Ho, Filippenko, & Sargent (1997) separation between LINERs and TOs, our LINER-like sample defined using EW([OII])/EW(Hα) contains 88.4% LINERs, 8.6% TOs, 1.9% Seyferts, and 1.1% star forming galaxies.

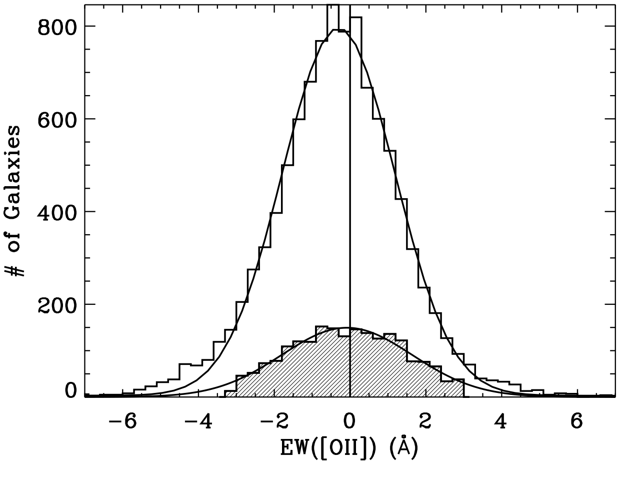

Fig. 3.— Histogram of [OII] EW in the quiescent galaxy sample. The unfilled histogram shows all galaxies that meet the selection criteria of §2.1. From these galaxies, a sub-sample of 2000 quiescent galaxies is chosen for comparison with the weak and strong LINER-like samples. The sub-sample, shown as the filled histogram, is constructed to have a symmetric gaussian distribution around EW([OII]) = 0, and is truncated at ±3.12 Å(the 2σ spread of the total EW([OII]) distribution) to limit contamination from undetected faint emission lines. See §2.3 for details.

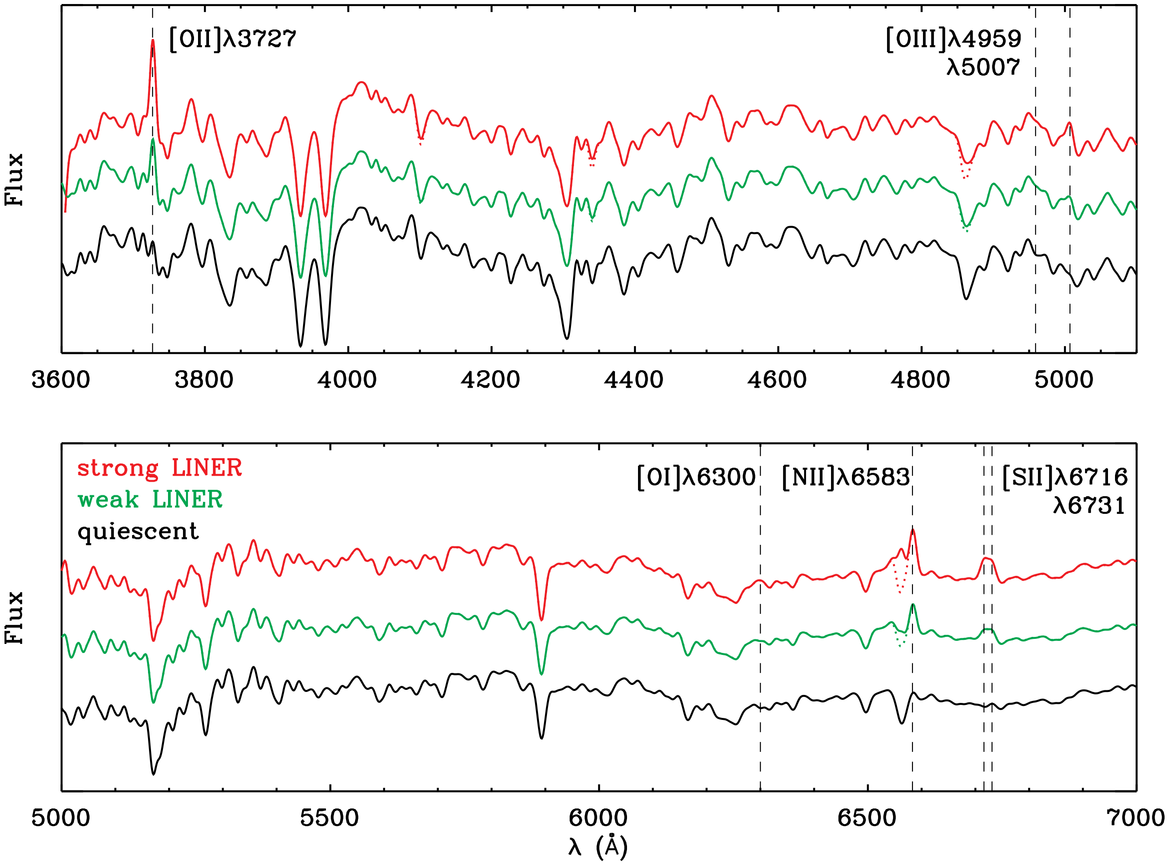

Fig. 4.— Stacked spectra for the galaxy bins with $70 < \sigma < 120$ km s^{-1} (the lowest σ bins), with and without emission infill corrections. The black, green, and red lines show the quiescent, weak LINER-like, and strong LINER-like galaxy bins, respectively. Solid lines show the uncorrected spectra, while dotted lines show the emission infill correction. Differences are only visible in the Balmer lines where the corrections have been made. The correction to Hδ in particular is very small. Strong emission lines are indicated by vertical dashed lines and are labelled. Except for the emission lines, the spectra are remarkably similar. This illustrates the extremely high S/N of the stacked spectra and shows the wealth of information in the absorption features, as well as the subtlety of the spectral variations that are quantified in this paper.

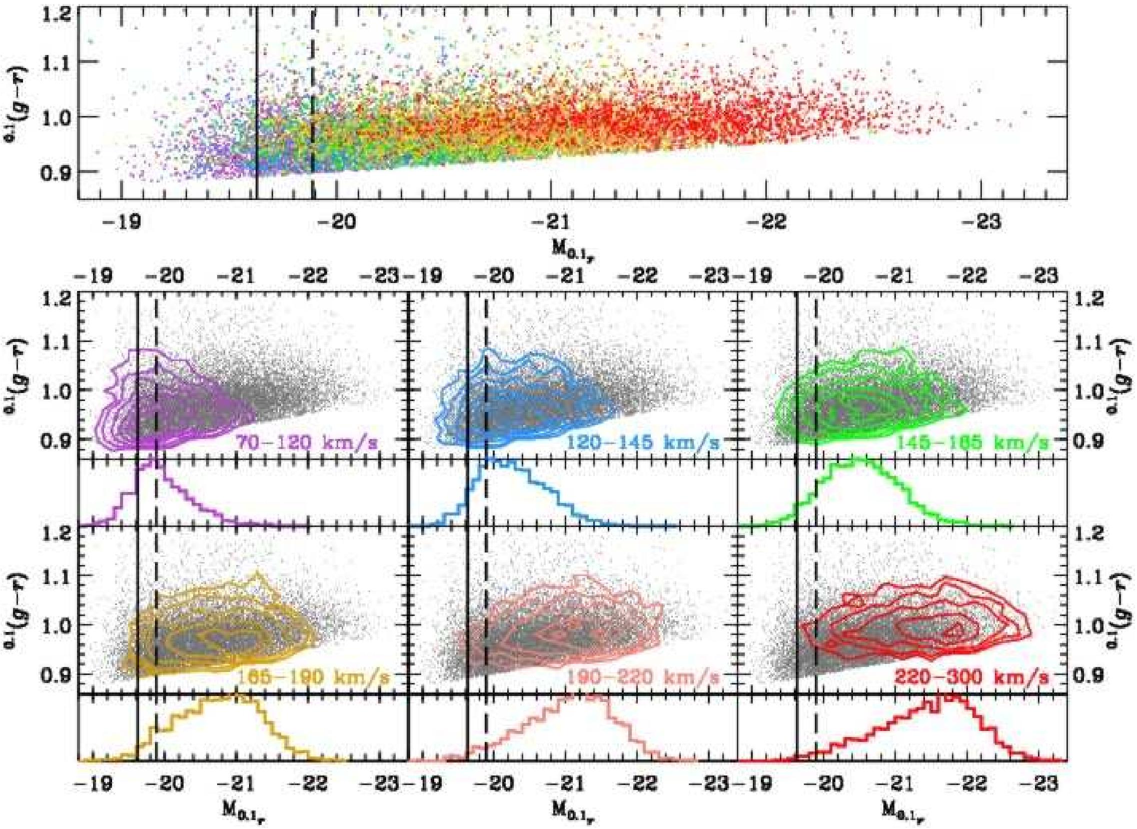

FIG. 5.— Color-magnitude diagrams (CMDs) of quiescent and LINER-like red sequence galaxies. The top panel shows the CMD of all (quiescent and LINER-like) galaxies in the sample color-coded by aperture-corrected velocity dispersion (σ): σ = 70–120 km s^{-1} in purple, σ = 120–145 km s^{-1} in blue, σ = 145–165 km s^{-1} in green, σ = 165–190 km s^{-1} in gold, σ = 190–220 km s^{-1} in salmon, and σ = 220–300 km s^{-1} in red. The lower panels show similar CMDs with all galaxies in gray and overplotted colored contours for the distribution of the σ range indicated. Colors correspond to the colors in the top panel. Below each contoured CMD is a histogram of the magnitude distribution of galaxies in that σ bin. In all panels, the black dashed line shows the 100% completeness limit, while the solid black line shows the magnitude at which the sample is 50% incomplete. The histograms show that the highest σ bins are effectively complete while the lower σ bins are seriously incomplete. A correction for this effect is described in §A. Higher σ galaxies are more luminous and redder than lower σ galaxies, but there is a large spread in both magnitude and color at fixed σ, typically larger than the separation between σ bins. At fixed σ, there is no clear color-magnitude relation.

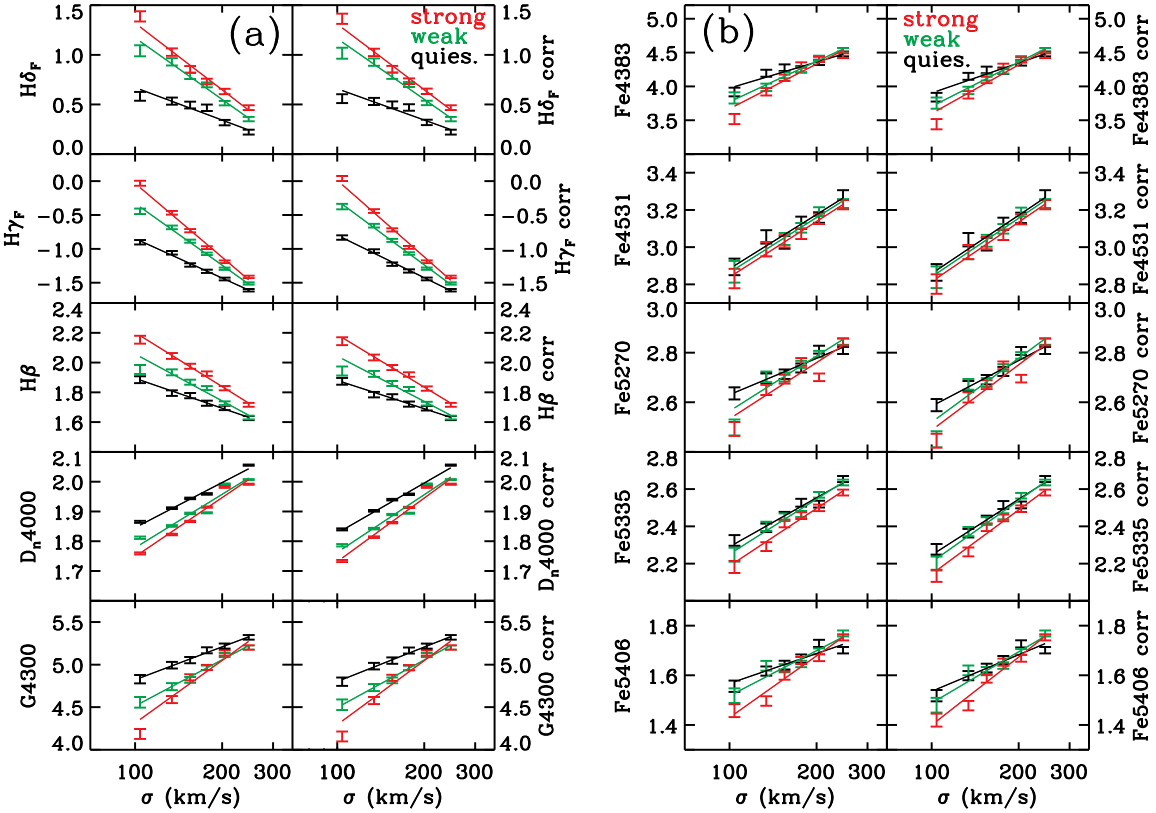

Fig. 6.— Lick index measurements in the stacked spectra as a function of the mean σ and emission line properties of the galaxies in each stacked spectrum. Quiescent galaxies are shown in black, weak LINER-like galaxies in green, and strong LINER-like galaxies in red. Error bars show the 1σ line strength measurement errors. Solid lines show linear least-squares fits of index strength onto σ, independently for each bin in emission line properties. (a) Indices strongly sensitive to age. (b) Indices dominated by iron absorption lines. In each panel, the left column shows raw measured indices, while the right column shows the indices corrected for incompleteness in the lower σ bins (see §A). The Balmer line strengths decrease with increasing σ while all other line strengths increase with increasing σ. This is consistent with higher σ galaxies being older and/or more metal rich than lower σ galaxies. Galaxies with LINER-like emission have stronger Balmer lines and weaker metal lines, consistent with LINER-like galaxies having younger age and/or lower metallicities than quiescent galaxies. (c) and (d) Indices strongly affected by non-solar abundance ratios. The same trends are visible as in panel (b), that higher σ galaxies have stronger absorption lines than lower σ galaxies while LINER-like galaxies have weaker absorption lines than quiescent galaxies (with the exception of Na D, where LINER-like galaxies have stronger absorption than quiescent galaxies; see §3.2 for details).

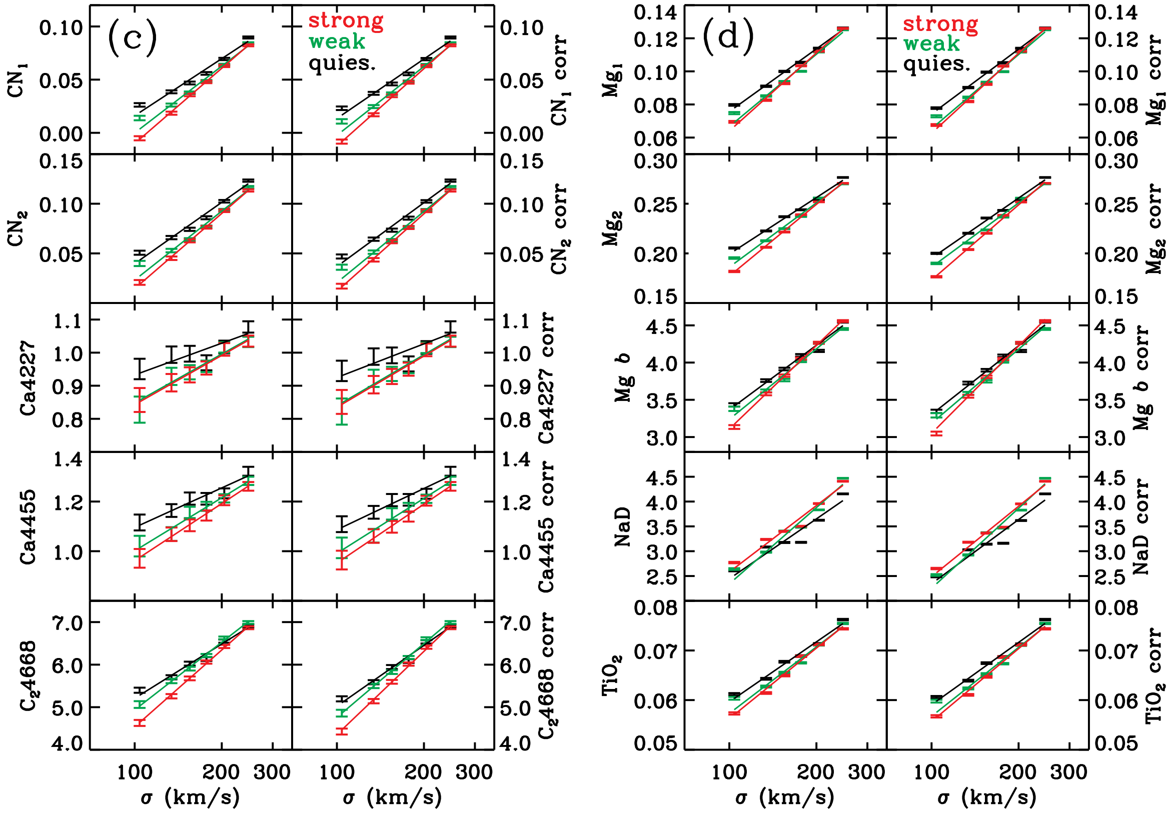
(c)
(d)
strong
weak
quies.
CN$_1$
CN$_1$ corr
CN$_2$
CN$_2$ corr
Ca4227
Ca4227 corr
Ca4455
Ca4455 corr
C$_2$4668
C$_2$4668 corr
Mg$_1$
Mg$_1$ corr
Mg$_2$
Mg$_2$ corr
Mg b
Mg b corr
NaD
NaD corr
TiO$_2$
TiO$_2$ corr
0.10
0.05
0.00
0.15
0.10
0.05
1.1
1.0
0.9
0.8
1.4
1.2
1.0
7.0
6.0
5.0
4.0
0.14
0.12
0.10
0.08
0.06
0.30
0.25
0.20
0.15
4.5
4.0
3.5
3.0
4.5
4.0
3.5
3.0
2.5
0.08
0.07
0.06
0.05
100
200
300
σ (km/s)

FIG. 6.— cont.

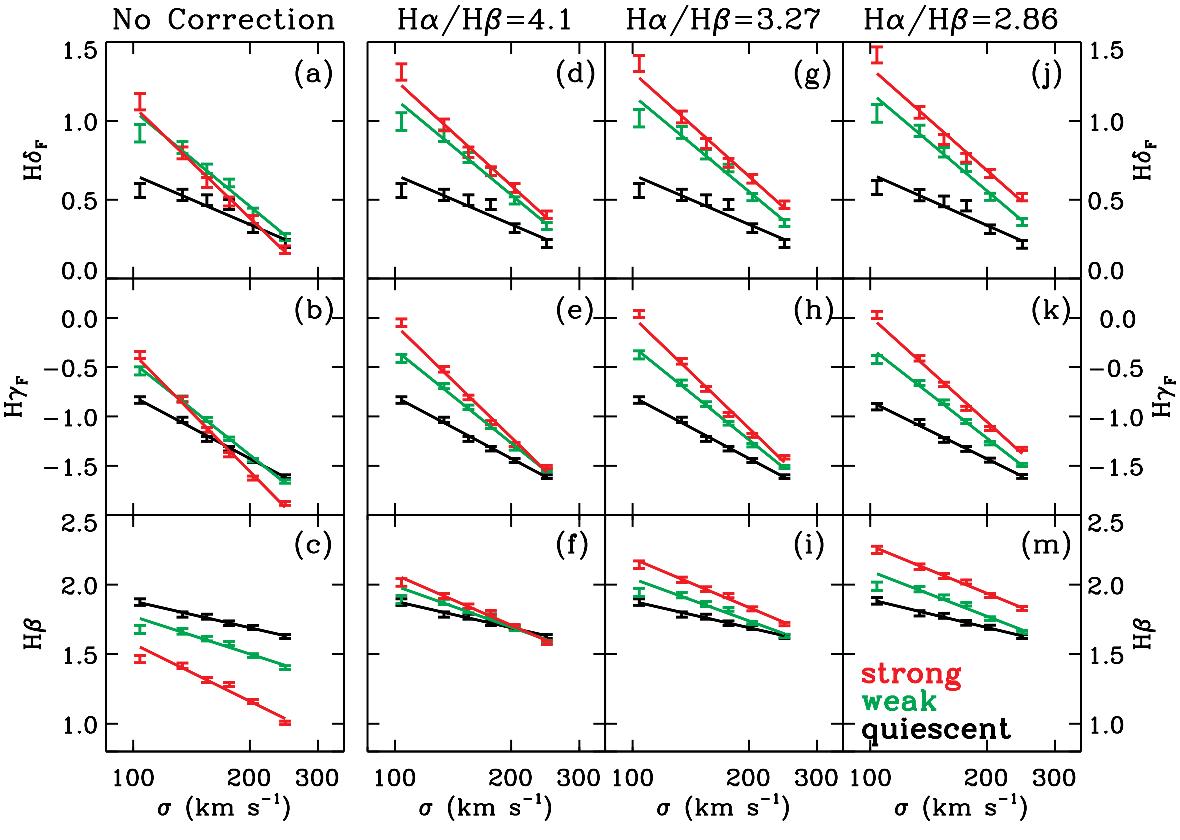

FIG. 7.— The effect of emission infill and various corrections for emission infill on Balmer absorption line strengths. As before, quiescent galaxies are shown in black, weak LINER-like galaxies in green, and strong LINER-like galaxies in red; error bars show measurement errors for the stacked spectra, and solid lines are linear least squares fits of line strength onto σ. (a–c) Balmer absorption line measurements with no infill correction applied. Note that in (c) Hβ is substantially filled in by emission in the LINER-like galaxies while in (a) Hδ_F is only marginally affected. Panels (d–m) show the effects of making a range of reasonable emission infill corrections. (d–f) show the Balmer lines when the Balmer decrement measured by Yan et al. (2006) is used. Hβ line strengths vary little between quiescent and LINER-like galaxies, while Hδ_F line strengths vary substantially. (g–i) show the Balmer lines using the Balmer decrement measured in red sequence LINERs of Ho, Filippenko, & Sargent (1997). These two choices of the Balmer decrement likely bracket the true mean value of the Balmer decrement in these systems. (j–m) show the Balmer lines using a "maximal" Balmer decrement, with Hα/Hβ characteristic of stellar-ionized HII regions and no reddening. The trend of stronger Balmer absorption in LINER-like galaxies exists for all reasonable values of the Balmer decrement, and exists even in the uncorrected Hδ_F, where emission infill is minimal.

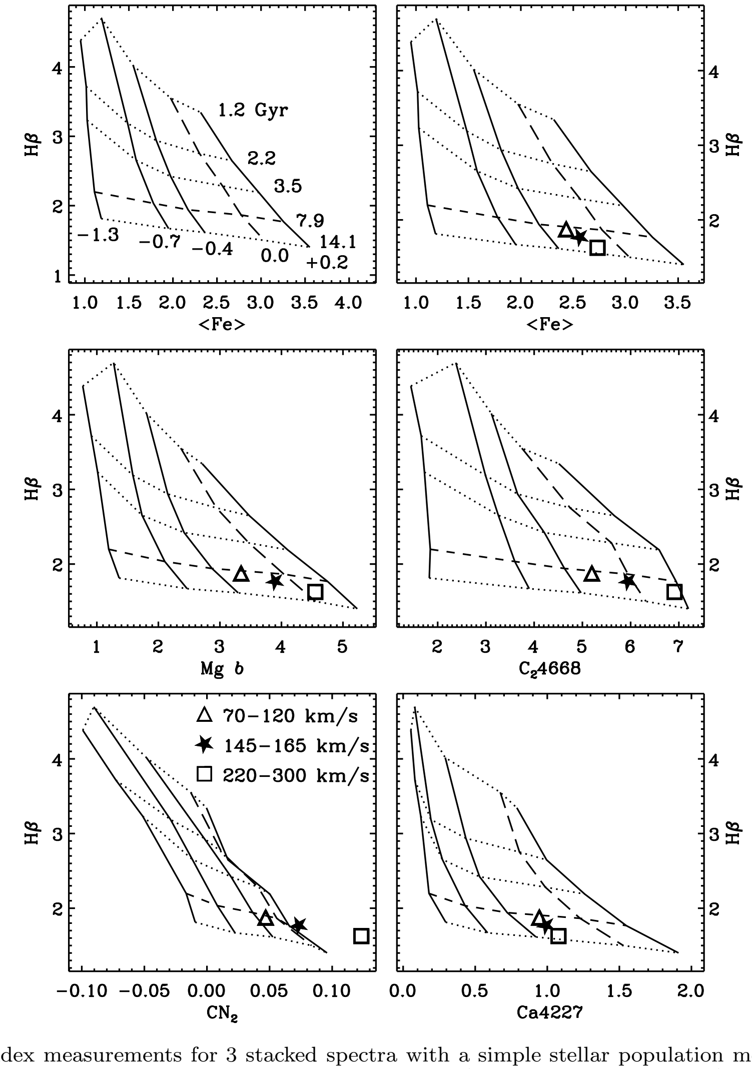

Fig. 8.— Comparison of Lick index measurements for 3 stacked spectra with a simple stellar population model from Schiavon (2007). The triangle, star, and square, show measurements for the $70 < \sigma < 120$ km s^{-1}, $145 < \sigma < 165$ km s^{-1}, and $220 < \sigma < 300$ km s^{-1} quiescent galaxy bins, respectively. Solid lines connect models of the same [Fe/H], from left to right: −1.3, −0.7, −0.4, 0.0, and +0.2. Dotted lines connect models of the same age, with ages from top to bottom: 1.2, 2.2, 3.5, 7.9, and 14.1 Gyr, as labelled in the top left plot. For reference, the [Fe/H] = 0.0 and *age* = 7.9 Gyr lines are shown as the long-dash and short-dash lines, respectively. The model has abundance ratios [Mg/Fe] = [Na/Fe] = [Si/Fe] = [Ti/Fe] = 0.120, [C/Fe] = 0.100, [N/Fe] = −0.002, and [Ca/Fe] = 0.010, calculated with a solar isochrone and with [O/Fe] = [Cr/Fe] = 0.0. This is the best-fitting model for the $70 < \sigma < 120$ km s^{-1} data (triangle), as determined by **EZ_Ages** (Graves & Schiavon 2007). Note that the data points for the $70 < \sigma < 120$ km s^{-1} stacked spectrum fall at the same values of *age* and [Fe/H] in each panel, as expected since this model gives consistent parameters for all indices. The data points from the $145 < \sigma < 165$ km s^{-1} (star) and $220 < \sigma < 300$ km s^{-1} (square) stacked spectra do *not* fall at the same values in each panel; higher values of [Mg/Fe], [C/Fe], and [N/Fe] are needed to make the age and [Fe/H] measured in Mg *b*, $C_2$4668, and CN_2 match the other panels, suggesting that the higher σ galaxies are enhanced in [Mg/Fe], [C/Fe], and [N/Fe] over the $70 < \sigma < 120$ km s^{-1} galaxies.

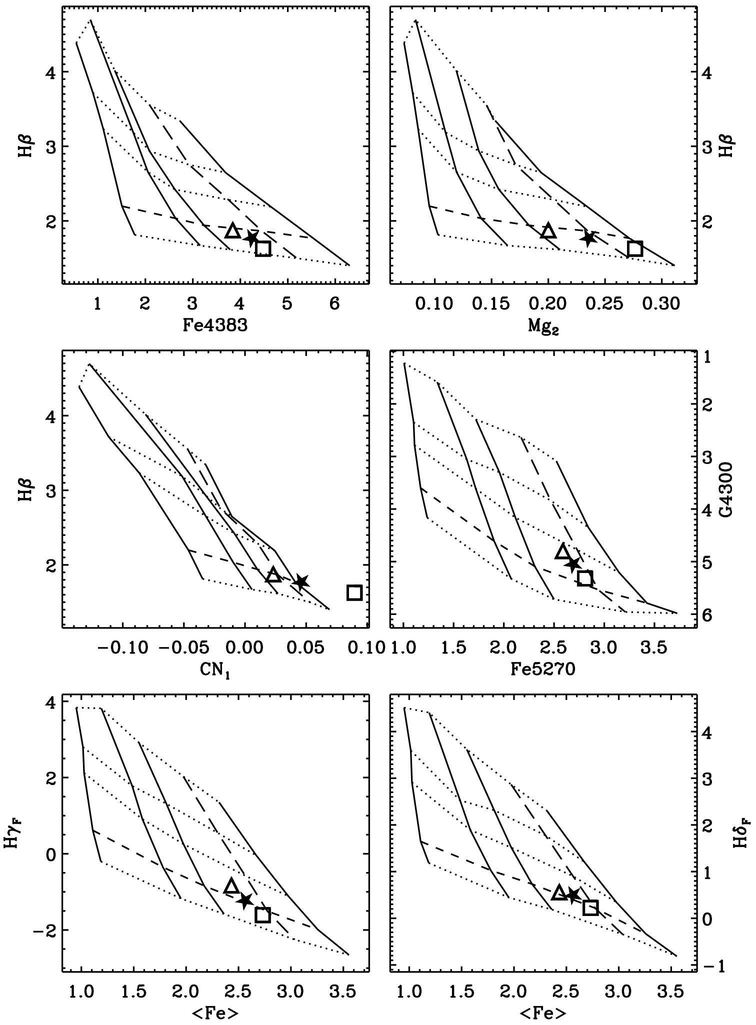

FIG. 9.— Index-index plots for indices *not* used by **EZ_Ages** (Graves & Schiavon 2007) in the abundance fitting process. All lines and symbols are as in Figure 8. The *age* and [Fe/H] values for the $70 < \sigma < 120$ km s^{-1} galaxies (triangle) are in good agreement with those seen in Figure 8, with the exception of G4300 and Hγ_F. Also, the higher σ galaxies have stronger Mg$_2$ and CN$_1$ than predicted by this model, suggesting they have higher [Mg/Fe], [C/Fe], and [N/Fe] than the $70 < \sigma < 120$ km s^{-1} galaxies, as was also implied by Figure 8.

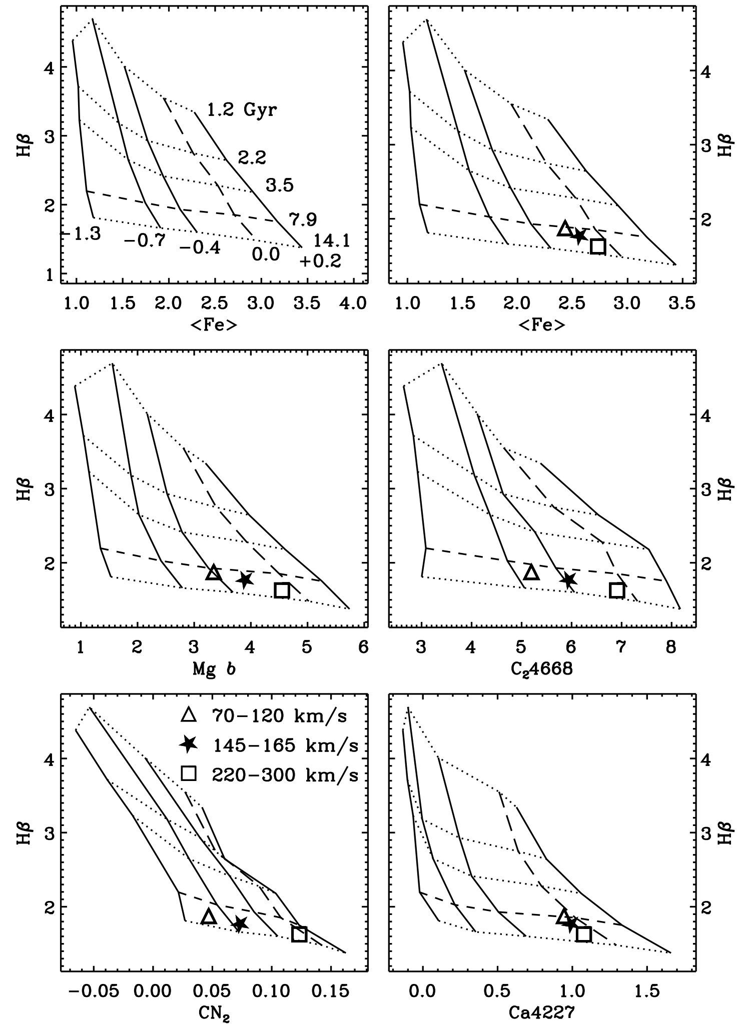

FIG. 10.— Same as Figure 8 except that grids are computed using the best-fit abundances for the quiescent $220 < \sigma < 300$ km s^{-1} data, as determined by **EZ_Ages**. This model has [Mg/Fe] = [Na/Fe] = [Si/Fe] = [Ti/Fe] = 0.260, [C/Fe] = 0.270, [N/Fe] = 0.220, and [Ca/Fe] = 0.040, calculated with a solar isochrone and with [O/Fe] = [Cr/Fe] = 0.0. The triangle, star, and square show the data for the $70 < \sigma < 120$ km s^{-1}, $145 < \sigma < 165$ km s^{-1}, and $220 < \sigma < 300$ km s^{-1} quiescent stacked spectra, respectively. Here, note that the data point for the $220 < \sigma < 300$ km s^{-1} stacked spectrum falls in the same position on the grid in each index-index plot, indicating that this is the correct abundance pattern for this data. The lower σ galaxies, by contrast, are clearly less enriched in Mg, CH, and CN than this model as shown by their location in the plots of Hβ against Mg *b*, $C_2$4668, and CN$_2$.

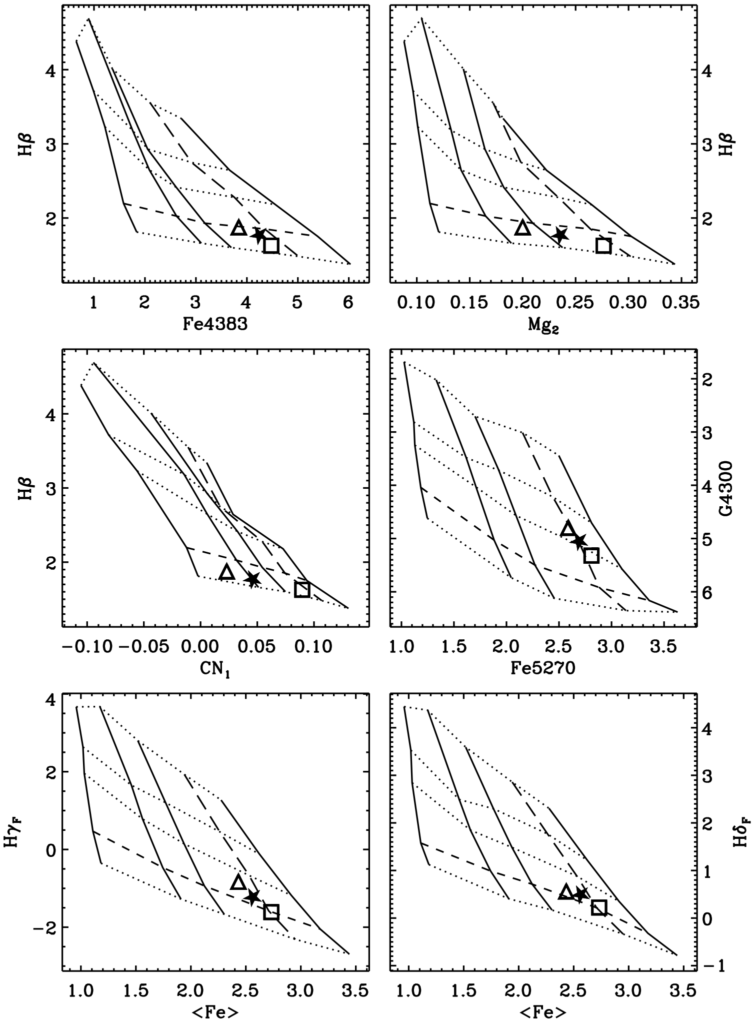

FIG. 11.— Same as Figure 9 except that grids are computed using the best-fit abundances for the quiescent $220 < \sigma < 300$ km s^{-1} data, showing indices not used in the fitting process. The plots of Hβ against Fe4383, Mg$_2$, and CN$_1$ give ages and [Fe/H] values for the $220 < \sigma < 300$ km s^{-1} data which are consistent with those in Figure 10, indicating that this abundance pattern reproduces even indices which are not used in the fitting process. The G4300 index is inconsistent with other indices, as discussed in the text. The ages measured from Hγ_F and Hδ_F are slightly younger than the ages measured from Hβ.

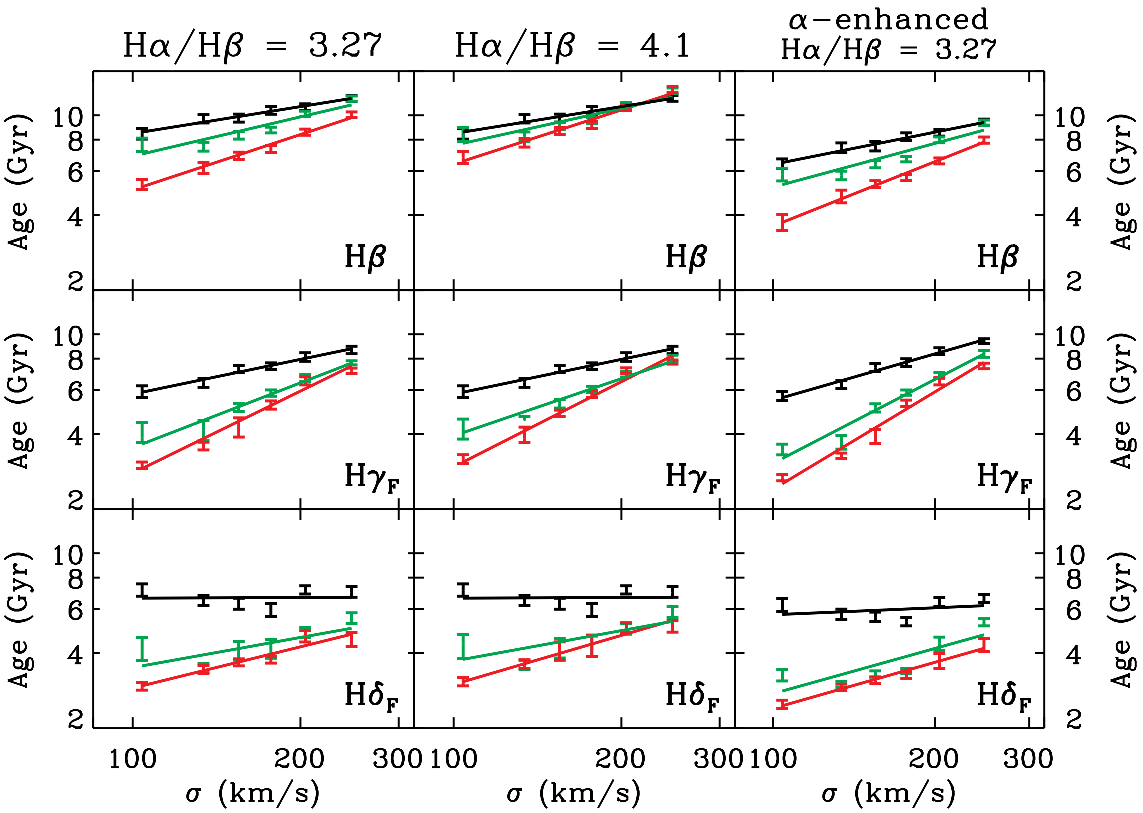

Fig. 12.— SSP ages as a function of σ and emission line properties. As in previous plots, quiescent, weak, and strong LINER-like galaxies are shown in black, green, and red, respectively. Error bars show the uncertainty in the ages due to measurement errors in the Balmer lines and $\langle$Fe$\rangle$ index only. Solid lines show linear least squares fits of age onto σ for each data set. Ages are determined separately for the three Balmer lines Hβ, Hγ_F, and Hδ_F. The left and center columns show the ages measured with the Ho, Filippenko, & Sargent (1997, our preferred correction) and Yan et al. (2006) Balmer decrements, respectively, to illustrate the effect of different infill corrections. Both are determined by **EZ_Ages** (Graves & Schiavon 2007) using a solar-scale isochrone. The right column shows the effect on the age measurements when an α-enhanced isochrone and [O/Fe] = +0.3 are adopted. Higher σ galaxies have older ages than lower σ galaxies, and LINER-like galaxies are younger than quiescent galaxies at fixed σ, independent of the choice of Balmer decrement, stellar population model isochrone, or Balmer line used to make the measurement. However age differences are more pronounced using higher-order Balmer lines, as expected if the stellar populations have a *distribution* of ages. A smaller Balmer decrement (i.e., larger infill correction) leads to larger differences between LINER-like and quiescent ages. The use of an α-enhanced isochrone produces systematically younger ages in Hβ, but qualitatively similar trends with σ and emission line properties.

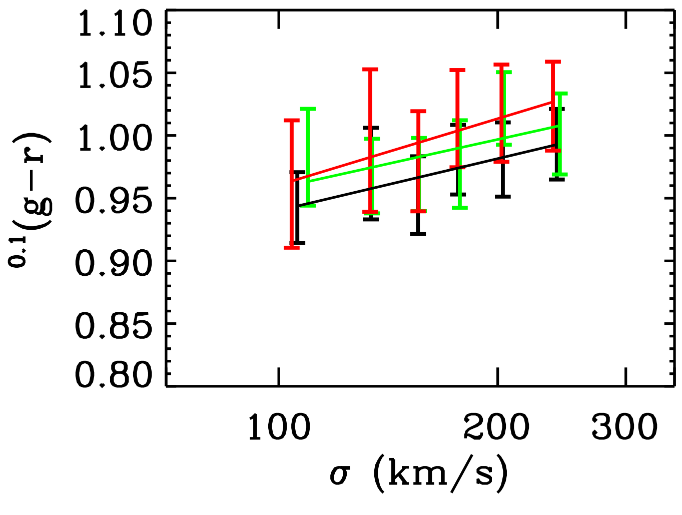

FIG. 13.— Median $^{0.1}(g-r)$ colors as a function of mean σ for the galaxies that went into each stacked spectrum. The quiescent galaxies are shown in black, the weak LINER-like galaxies in green, and the strong LINER-like galaxies in red. Solid lines show a linear least-squares fit of color onto log σ. The error bars show the 1σ spread in the color values for each bin of galaxies. Although the spectral data show that the LINER-like galaxies are typically *younger* than their quiescent counterparts, the LINER-like galaxies on average have slightly *redder* colors. This is not a metallicity effect (see Figure 14) but is probably an indication that the LINER-like galaxies are typically more dust-reddened than the quiescent galaxies, consistent with the larger amounts of interstellar NaD absorption seen in the LINER-like galaxies in Figure 6. See §5.1 for details.

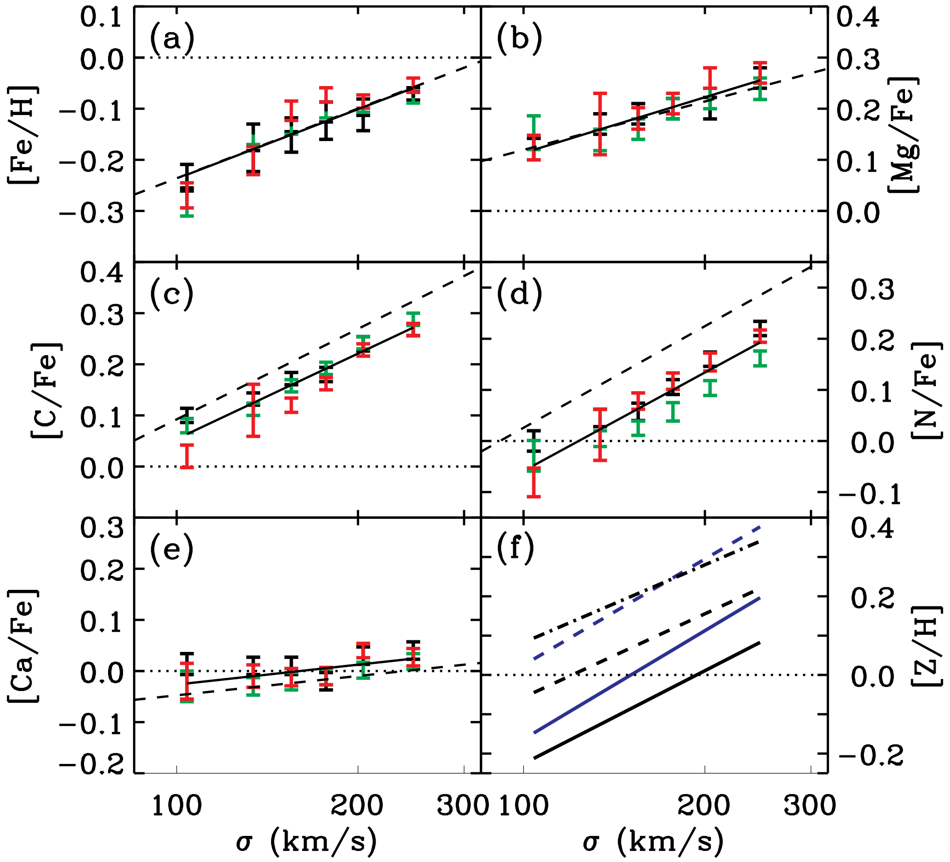

Fig. 14.— (a–e) [Fe/H] and abundance ratios for quiescent and LINER-like galaxies as a function of σ. Quiescent, weak, and strong LINER-like galaxies are shown in black, green, and red, respectively. Error bars show the uncertainties in each abundance due to measurement errors in the Lick indices as described in §5.3. The dotted line in each panel shows solar abundance. There are no significant variations in abundances or abundance ratios between quiescent and LINER-like galaxies. The solid line show a linear least squares fit of abundance onto σ for quiescent and LINER-like galaxies simulatenously. Abundances are computed using a solar-scale isochrone and assuming [O/Fe] = 0.0, with Na, Si, and Ti set to track Mg, and [Cr/Fe] = 0.0. The abundances computed using the α-enhanced isochrone are not significantly different. The dashed line shows the effect of computing abundances with [O/Fe] = +0.3. All abundances increase with σ, [Fe/H], [C/Fe], and [N/Fe] most strongly. All galaxies are Mg-enhanced. (f) Linear least squares fits of [Z/H] as a function of σ. The black solid, dashed, and dash-dot lines show [Z/H] computed assuming [O/Fe] = 0.0, [O/Fe] = +0.3, and [O/Fe] = +0.5, respectively. The blue solid and dashed lines show [Z/H] computed assuming [O/Fe] = [Mg/Fe], and [O/Fe] = [Mg/Fe] + 0.3, respectively. Total metallicity is dominated by [O/Fe] which cannot be measured and is thus highly uncertain.

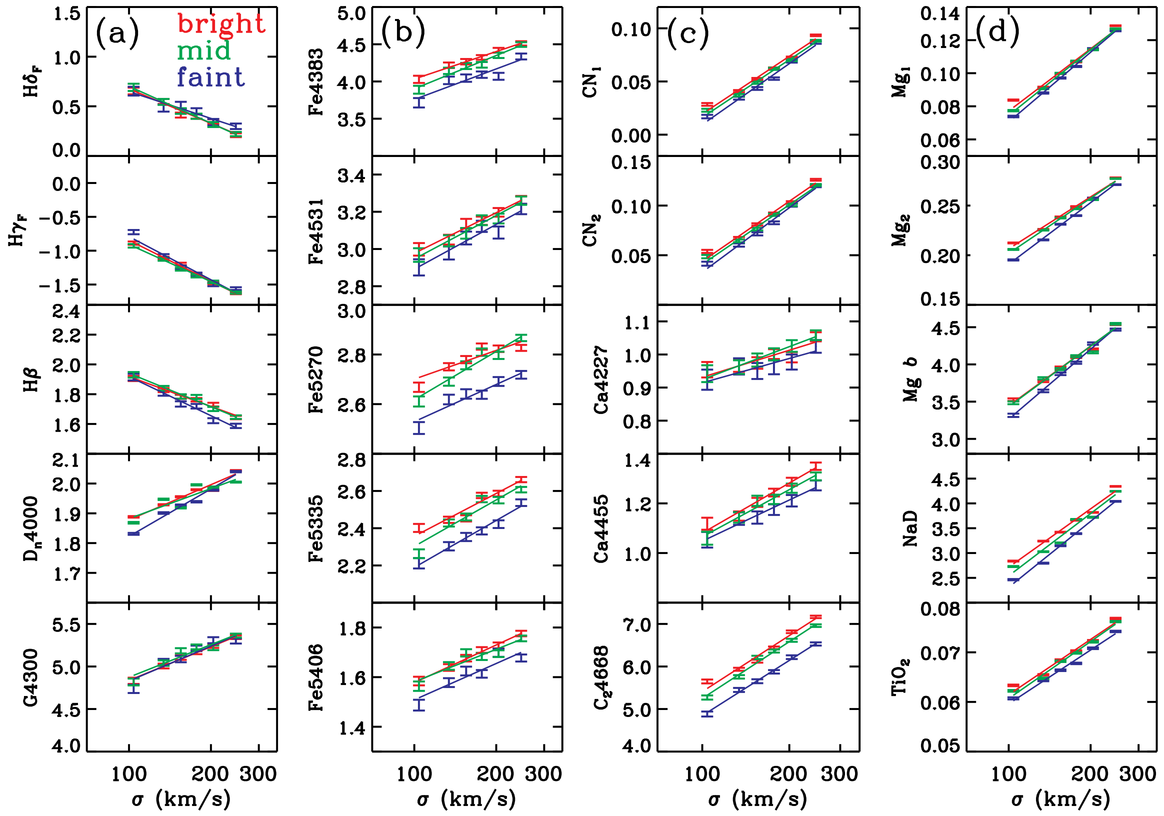

FIG. 15.— Lick index line strengths in stacked spectra of quiescent red sequence galaxies, as a function of σ and magnitude. Each bin in σ has been divided into faint, mid-magnitude, and bright sub-bins, with equal numbers of galaxies in each sub-bin. The faintest galaxies at each σ are shown in blue, the mid-magnitude galaxies are shown in green, and the brightest galaxies are shown in red. Error bars show the 1σ index measurement errors for each stacked spectrum. Solid lines show linear least-squares fits of index strength onto σ, independently for each bin in magnitude. As in Figure 6, panel (a) shows strongly age-sensitive indices, panel (b) shows indices dominated by iron absorption lines, and panels (c) and (d) show indices that are sensitive to non-solar abundance ratios. Faint galaxies appear to have similar ages but lower metal abundances when compared to mid-magnitude and bright galaxies at the same σ.

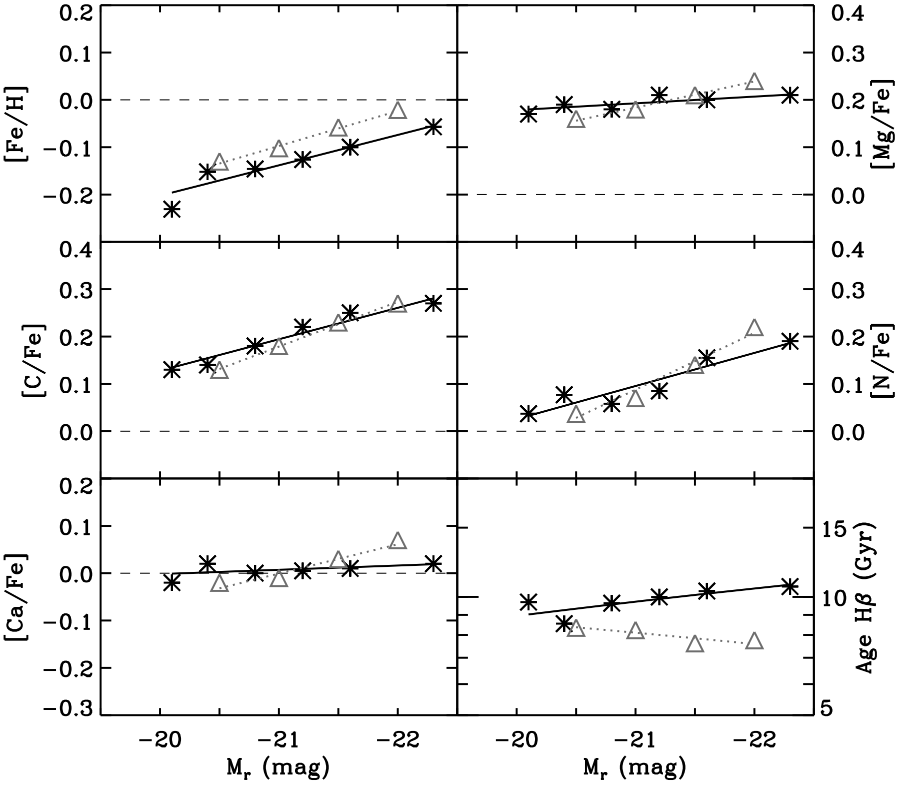

FIG. 16.— [Fe/H], abundance ratios, and ages of stacked spectra, as a function of galaxy absolute magnitude. Black stars are the luminosity-binned data from appendix B. Only the stacked spectra for quiescent galaxies are shown. The solid black line shows a linear least-squares fit of the stellar population parameter onto magnitude for the luminosity-binned data. Grey triangles show the results from Schiavon (2007) for the Eisenstein et al. (2003) stacked spectra. The dotted grey line shows a linear least-squares fit for the Eisenstein et al. (2003) stacked spectra. Solar abundance and abundance patterns are shown for reference as the dashed line in each panel. The Eisenstein et al. (2003) data (triangles) show younger ages, slightly higher [Fe/H], and slightly steeper abundance relations versus magnitude than do the luminosity-binned spectra from our sample (stars).

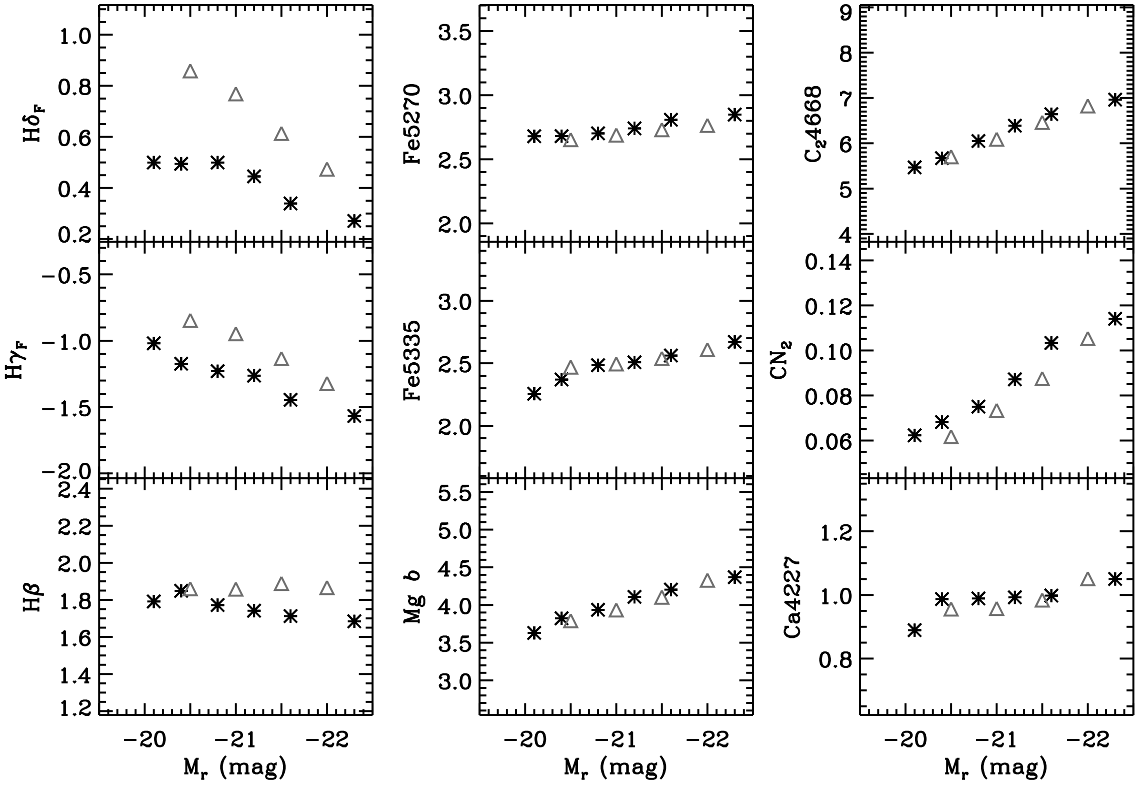

FIG. 17.— Selected Lick index line strengths as a function of galaxy magnitude. Black stars are the luminosity-binned data from appendix B. Only the stacked spectra for quiescent galaxies are shown. Grey triangles show indices measured in the Eisenstein et al. (2003) stacked spectra. In both samples, Balmer lines weaken as galaxy luminosity increases with the exception of Hβ, which behaves similarly to Hδ_F and Hγ_F in our data but is constant in the Eisenstein et al. (2003) data. Hδ_F and Hγ_F are stronger in the Eisenstein et al. (2003) data than in ours, consistent with younger mean ages. In contrast to the Balmer lines, the other Lick indices are very similar between the two data sets. The metal lines may be slightly weaker in the Eisenstein et al. (2003) data than in ours, again consistent with younger ages. The consistency of the metal absorption line strengths between the two samples implies that the differences in the measured abundance trends seen in Figure 16 are caused by the difference in measured Balmer line strengths, rather than intrinsic differences in metallicity.